2026-06-10

Evaluating C-Band Scatterometer Images for Estimating Deforestation in the Amazon Rainforest

Alex McBride
Brigham Young University

Evaluating C-Band Scatterometer Images for Estimating Deforestation in the Amazon Rainforest

Alex McBride

A thesis submitted to the faculty of
Brigham Young University
in partial fulfillment of the requirements for the degree of

Master of Science

David G. Long, Chair
Preston Manwaring
Willie Harrison
Rex Nielson

Department of Electrical and Computer Engineering

Brigham Young University

Evaluating C-Band Scatterometer Images for Estimating Deforestation in the Amazon Rainforest

Alex McBride
Department of Electrical and Computer Engineering
Master of Science

BYU Engineering

Abstract

Satellite-based active microwave sensors have been successfully employed for a wide range of vegetation and soil studies. Spaceborne microwave instruments have proven particularly useful for wide-scale monitoring of the vegetation, especially under conditions that limit the effectiveness of high-resolution optical sensors. Satellite scatterometry can be used to detect and model deforestation in the Amazon rainforest by correlating changes in the C-band backscatter data to observed changes in vegetation coverage.

The exploratory methodology developed in this paper applies the longest continuous microwave satellite record to the problem of deforestation. The backscatter measurements taken by the ERS and ASCAT missions provide more than 30 years of data that has been successfully applied to classify vegetation on a global scale. This research investigates the effectiveness of C-band scatterometer data for detecting anthropogenic changes in rainforest and grassland vegetation, opening the possibility for microwave-based historical deforestation records.

Keywords: deforestation, Amazon rainforest, C-band scatterometer, remote sensing, estimation

Acknowledgments

My thanks go out to my wife Joanna, first and foremost, for her constant support and confidence in me.

To my parents, siblings, and grandparents, for believing in me and my ideas.

To Dr. Long and my friends at the MERS lab, for always teaching me something new, and to my committee for being part of the journey.

And finally, to Lauren and Nick Bringhurst, for showing me that the world is beautiful because of the people in it.

Table of Contents

List of Figures

List of Tables

Nomenclature

α	Detection Rate
β	False Positive Rate
δ	Deforestation Percentage
λ	Wavelength
σ^0	Sigma Naught
AC	Acre
Af	Tropical Rainforest Climate
AM	Amazonas
Am	Tropical Monsoon Climate
AMI	Active Microwave Instrument
ASCAT	Advanced Scatterometer
Aw	Tropical Savanna (Dry Winter) Climate
DETER	Real-Time Deforestation Detection System
ERS	European Remote-Sensing Satellite
ESA	European Space Agency
GIS	Geographic Informational System
INPE	National Institute of Space Research
MERS	Microwave Earth Remote Sensing
MetOp	Meteorological Operation satellite
MODIS	Moderate Resolution Imaging Spectroradiometer
MT	Mato Grosso
NDVI	Normalized Daily Vegetation Index
PA	Pará
PRODES	Amazon Forest Monitoring Program
RAISG	Amazon Network of Georeferenced Socio-Environmental Information
RR	Roraima
SAR	Synthetic Aperture Radar
SCIRoCCo	Scatterometer Instrument Competence Centre
UHR	Ultra-High Resolution

1 Introduction

Today, forests around the world face threats from a wide variety of sources. The environmental pressures of agriculture, mining, wildfires, and international trade are particularly acute in developing countries. Brazil, Madagascar, Indonesia, the Congo, and other countries in the tropics are experiencing deforestation at an increasing rate, owing in part to the economic consumption of developed nations [1]. The loss of tropical forests is a matter of global concern due to landscape degradation's negative impacts on worldwide water and carbon cycles, weather patterns, and biodiversity. Over the past several decades, measuring and monitoring deforestation has become key to understanding environmental changes that impact both rich and poor countries alike [2].

The Amazon rainforest accounts for roughly half of Earth's tropical forested area [1] and is the most extensively researched rainforest biome. Studies of the ecological, environmental, and social impacts of deforestation in this region have been enabled by the widening array of Earth remote sensing satellites collecting continuous data on the distribution and health of the Amazon [3][4]. Due to the proliferation and sophistication of both optical and microwave sensors in space, it is now possible to detect many deforestation events within one or two days [5] provided appropriate monitoring is taking place [6]. The timeliness of modern deforestation alerts is useful not just for environmental policy enforcement, but also for understanding the trends and forces that drive tropical habitat loss.

Whereas near real-time detection is attainable now, past optical satellite monitoring projects were limited in their ability to quickly identify deforestation. Thus, it was only possible to make total deforestation estimates on an annual basis [5], which limited the ability to study temporal patterns of deforestation. Due to limitations of the sensors used at the time, these early records also were subject to atmospheric conditions, restricting the ability to detect deforestation in certain areas of the Amazon due to consistent cloud cover [6].

This thesis aims to ameliorate these deficiencies by using C-band microwave sensor data to estimate historical Amazon deforestation at a finer time scale. In this observational study, data from two active microwave satellites spanning from 1991 to the present are used in conjunction with high-resolution deforestation tracking to demonstrate the impact of landscape degradation on microwave backscatter and estimate deforestation area using C-band scatterometer data.

While only a preliminary study into the application of microwave scatterometry for estimating tropical deforestation, this analysis has the potential to augment existing records of the Amazon rainforest by providing finer temporal resolution coverage than that used in prior deforestation measurements of this time period. Additionally, the methods in this paper may be further developed to create estimates for deforestation over time in understudied tropical regions beyond the Amazon.

1.1 People and Ecology of the Amazon

It would be remiss to neglect both the human and ecological aspects of the Amazon region, as it is home to remarkable natural and cultural diversity. This section serves to provide context for the trends of land use and protection discussed later on, but it also seeks to recognize the intrinsic value of the landscape beyond the technical analysis.

The Amazon is home to some of the most biodiverse regions in the world [7] [8] and comprises the largest rain forest on Earth [5]. Its biomes serve as a keystone to global carbon cycles, a home to tens of thousands of animal species, and thousands of useful plants [2] [9]. Beyond the rainforest, there are also multiple savanna biomes that make up parts of the Amazon basin such as the Cerrado, the Llanos and the Guianan savanna. These ecosystems bordering the Amazon rainforest face intense habitat loss as part of the "arc of deforestation" [5] and often go unrecognized as a facet of Amazonia's incredible biodiversity [10].

Indigenous peoples have inhabited the rainforest and surrounding savannas for 10,000-12,000 years [11], and are thought to have reached a peak population of roughly 5 million in the 16th century CE, prior to European colonization [7]. For thousands of years, people have flourished in the Amazon, making art and culture [12], building complex structures and society [7], and practicing sophisticated habitat management [11]. It has been found that through cultivation of desired trees and slash-and-burn agriculture, indigenous societies exerted a *positive* influence on biodiversity by creating niches where non-dominant plant and animal species could thrive [11].

In Brazil today, there are over 160 indigenous groups living in the Amazon speaking 195 languages. Many of these groups are actively involved in the protection of the natural environment and have been instrumental in the development of conservation policy [13]. Approximately 40 million people, including 1.5 million belonging to indigenous groups [14], live in the Amazon region, as well as a number of modern "traditional peoples" that reside in the forest and depend on it for survival [13].

In the Brazilian Amazon, there are 2.2 million km^2 of officially designated indigenous or ecological preserve lands, with an additional 700,000 km^2 of undesignated lands, where all clearing is illegal [15]. Thus, roughly 65% of the Brazilian Amazon's 4.4 million km^2 area is protected, meaning only limited economic clearing can legally take place therein. Illegal activity is, however, widespread and causes the vast majority of habitat loss in the Amazon [15].

Today, global deforestation is driven primarily by agriculture, with 86% attributed to crop and cattle production [2]. Approximately 14% of the total area of the Amazon has been replaced by cattle pasture and agricultural fields [14], primarily soy, cotton, and palm oil. Often, forest areas are illegally used for cattle grazing, then converted to cropland, after which reclamation by diverse rainforest vegetation is not possible.

Beyond land use for agriculture and the extraction of lumber, deforestation is driven by material interest in significant natural deposits of oil, gold, and minerals in Amazon soil[13] [14]. These economic forces have negatively influenced the enforcement of environmental policy and political commitment to the Amazon's protection, but global social and scientific efforts maintain the urgency of its preservation. Continually advancing sensors and tracking methodologies have led to an 85% reduction in the rate of Amazon deforestation since 2010 [15], a major success for remote sensing and for environmentalism.

2 Monitoring Deforestation

The current state of the art for monitoring deforestation utilizes moderate resolution optical imaging from a variety of satellites with increasing contributions from microwave satellites [4]. The Brazilian National Institute for Space Research (INPE) operates two notable programs monitoring deforestation known as PRODES and DETER which provide many years of comprehensive and reliable data on deforestation [5]. These programs rely primarily on optical sensors, one using data from an imaging satellite known as Landsat and the other data from a spaceborne sensor called the Moderate Resolution Imaging Spectroradiometer (MODIS). Both projects maintain active databases with distinct aims useful for studying deforestation.

2.1 PRODES

The PRODES dataset is the longest-running record of Amazon deforestation available, running from 1988 until the present. This project uses carefully selected Landsat images to measure the change in forest area with a high degree of accuracy. From the year the program began up to 2010, INPE measured an estimated 750,000 km^2 of vegetation suppression [5], accounting for approximately 17% of the land area of the Brazilian Amazon. Landsat's medium spatial resolution (30 m) imaging covers the Earth's surface over a period of 16 days. Images are generally selected from the dry season to minimize cloud coverage [16], though still suffer from limited visibility depending on atmospheric conditions during the imaging period [15][6]. The primary goal of PRODES is to measure deforestation area in a given year but is inadequate for real-time monitoring of deforestation events [5].

2.2 DETER

The second program, DETER, was developed to address the need for rapid response to landscape degradation from logging, mining, and fires. The DETER-A system began in 2004 using coarse resolution (250 m to 1 km) images from MODIS sensors, taking advantage of the 1 to 2 day global coverage that the sensor provides to create near-real-time alerts of deforestation. These alerts are used to direct law enforcement and environmental management efforts as needed to respond quickly when vegetation change is detected [17]. Originally, the minimum area detectable using the DETER system was 25 ha, but with the inclusion of a broader range of satellite-borne sensors this has been improved to a minimum area of 1 ha [6].

The coarse imaging resolution of the first stage of the DETER-A program prevented the system from providing real-time deforestation area estimates over the entirety of the Amazon. To address this limitation, further sensors were incorporated into the detection system in stages, the latest beginning in 2020 [3]. The current DETER-C program uses data from both MODIS and Landsat, optical data from European and Chinese imaging satellites, and synthetic aperture radar (SAR) images from the European Space Agency's Sentinel-1

satellites [6]. The variety of sensors permits vegetation change detection that is frequent and less dependent on atmospheric conditions than previous systems, though this data is not yet publicly available.

These two programs form the basis for both local enforcement of environmental policy and global studies of deforestation in the Amazon. PRODES has provided annual deforestation reports since 1988, quantifying the amount of deforestation and the effectiveness of policy enforcement during that year. DETER provides near real-time alerts for deforestation and describes the cause of particular events. Thus, PRODES and DETER are employed in this study to establish the ground truth for deforestation area and timing, and are compared to coarse-resolution microwave satellite images to develop timely estimates for historical deforestation.

3 Scatterometer Studies

3.1 Backscatter Mechanics

Spaceborne active microwave sensors, referred to as scatterometers, have been flown for geophysical data collection since 1978 [18]. A scatterometer works by transmitting a short pulse of microwave radiation at a determined frequency and measuring the amount of backscattered power that returns to the sensor. In microwave earth remote sensing, the amount of power received normalized for the area covered by the pulse is generally denoted as σ^0 ("sigma nought") or σ^0 brightness.

The power that returns to the sensor, known as backscatter, is influenced by both the physical properties of the surface being measured and the characteristics of the scatterometer's transmission. Surface roughness, the surface material's electromagnetic properties, azimuth and incidence angle, and wavelength all factor into the magnitude of microwave backscatter. Because a single scatterometer measurement covers many square kilometers of the Earth's surface, the reported σ^0 brightness is average backscatter over the surface area.

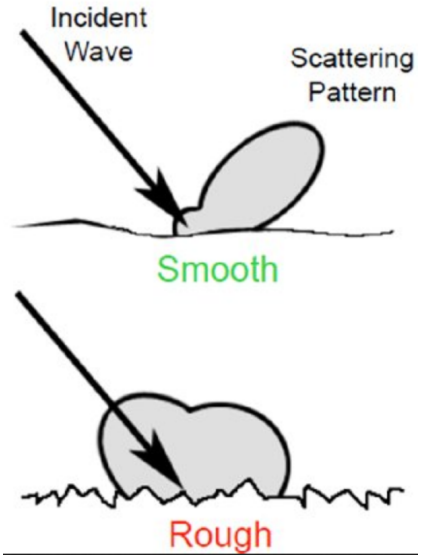

Figure 3.1: A visualization of the electromagnetic interaction of microwave energy with a smooth or rough scattering surface. The magnitude of energy returning to the transmitter (i.e. the satellite) is represented by the radius of the shape in the direction of the arrow. This demonstrates how a rough surface generally exhibits higher backscatter than a smooth surface, resulting in a higher σ^0 brightness. *Westerhoff, R. S., et. al. (2013). Automated global water mapping based on wide-swath orbital synthetic-aperture radar. Hydrology and Earth System Sciences, 17(2), 653.*

An individual scatterometer measurement contains the σ^0 brightness, the angle at which the pulse was transmitted towards the Earth's surface (incidence angle), the direction of

transmission (azimuth angle), and the exact time that measurement took place, along with several other attributes of the measurement. These measurements can be compared across space or time to generate a variety of different data types, such as a timeline of the σ^0 brightness of a single area over several years or a map of backscatter measurements in a set region during a single passover of the satellite. By aggregating information, wider trends become more apparent, though substantial effort is required to make meaningful conclusions about the area being studied.

Because measurements are being taken from a distance, the exact properties of the measurement area are unknown, but a carefully designed model is able to estimate those properties based on characteristics that are known (or can be inferred) and the behavior it exhibits under numerous measurements. For example, changes in vegetation can be estimated by correlating changes in vegetation backscatter over time with observed ecological disruption of the measurement area. This study explores the viability of C-band scatterometer data for modeling deforestation in the Amazon rainforest.

3.2 Microwave Radiation

Electromagnetic radiation is characterized by its frequency: how quickly the wave of light and energy oscillates. The distance between corresponding points in two consecutive cycles of the wave, which is called wavelength (λ) [19], can be calculated using the well-known equation

$$\lambda = c/f \tag{3.1}$$

where c is the speed of light and f is frequency.

Microwaves make up a range of frequencies from 1 GHz to 100 GHz, meaning that microwaves can have a wavelength from 30 cm at the lowest frequency to 3 mm at the highest. The wavelength a scatterometer uses determines what features it is sensitive to, as features that are roughly the same size or larger than their wavelength have stronger backscatter than smaller features. For example, ripples on the ocean's surface have a large impact on the magnitude of backscatter received at high frequencies, whereas at low frequencies large waves may dominate the backscatter.

Within this wide range of frequencies, microwaves are further divided into ranges called bands, each denoted by a letter [20]. Commonly-used bands in scatterometry include:

Band	Frequency	Wavelength
L	1-2 GHz	15-30 cm
C	4-8 GHz	3.75-7.5 cm
X	8-12 GHz	25-37.5 mm
Ku	12-18 GHz	16.7-25 mm

Table 3.1: Delineation of microwave bands commonly used in Earth remote sensing.

Besides frequency and wavelength, polarization is another notable element of electromagnetic interaction. An active sensor is generally designed to emit and detect electromagnetic waves whose oscillation is aligned in a single direction. In the context of earth remote sensing, emitted microwave energy either oscillates perpendicular or parallel to the surface of the Earth, which are respectively called vertical and horizontal polarization. A sensor designed for vertical polarization is described with the letters VV, meaning it emits and

receives vertically polarized electromagnetic waves. The same applies for HH sensors. A sensor may also be denoted as HV or VH, meaning it detects returning energy that changes polarization during its interactions. This is known as cross-polarization. Polarization determines which dimension of an object the radiation interacts with. If a microwave scatterometer is measuring backscatter over an area filled with tall, thin objects such as a corn field, the VV-polarized σ^0 is typically higher than the HH-polarized σ^0 measurement.

4 Active C-Band Satellite Systems

Though microwave scatterometers were originally developed for ocean wind speed estimation, these sensors show sensitivity to water in almost any environment. This sensitivity enables a variety of remote sensing applications beyond meteorology, including monitoring global ice volume, soil hydrology, and vegetation studies [18]. These satellites are designed to have frequent global coverage, enabling researchers to study long-term environmental trends across the globe. Since the inception of scatterometer remote sensing with NASA's SeaSat in 1978, scatterometers have found use in wind, ice, ocean, soil, and vegetation studies that benefit people around the world. This study uses data from satellites carrying two different scatterometer sensors: ERS and ASCAT.

4.1 ERS

The European Space Agency (ESA) launched their first scatterometer in 1991 with the aim of studying ocean wind patterns for meteorological forecasting. The European Remote Sensing (ERS) program launched two satellites carrying the Active Microwave Instrument (AMI), a 5.3 GHz VV-polarized microwave sensor capable of both scatterometry and SAR observations. These satellites, called ERS-1 and ERS-2, provide roughly 20 years of remote sensing data with wide applications in the fields of numerical weather prediction, soil hydrology, oceanography, and climate science [21][18].

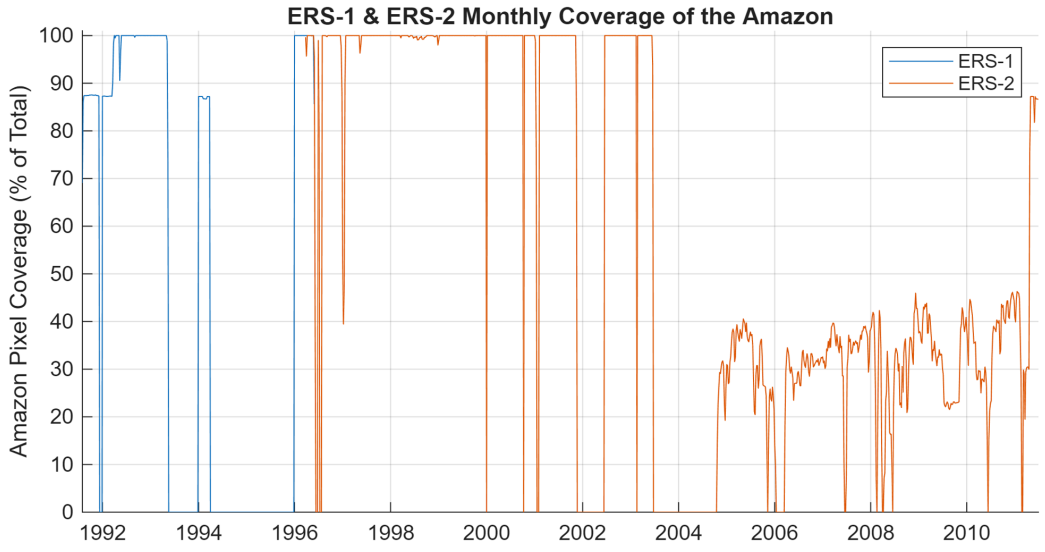

Figure 4.1: ERS scatterometer coverage of the Amazon basin. Up until 2004, dropouts are caused by failures experienced by the satellites or ground stations. After this point, SAR mode was heavily used, limiting the extent of scatterometer data. The northwestern Amazon was often measured using the scatterometer sensor for calibration purposes, providing a small level of coverage until the end of ERS-2's mission. ASCAT essentially achieves 100% coverage for its entire operating lifespan.

After ERS-2 was decommissioned in 2011, the body of ERS data was reprocessed to consolidate current best-known-methods for calibration and sensor characterization. The project, known as SCIRoCCo (Scatterometer Instrument Competence Centre) [22], provides intercalibrated data between ERS-1 and ERS-2 to account for sensor drift and increased the resolution of the raw measurements. Because of the calibration performed by SCIRoCCO, researchers have access to much higher-quality data than what was originally available during the operating lifespan of ERS. Additionally, this project delivered a report of missing data segments caused by raw data corruption, instrument unavailability, or ground station unavailability.

Data dropouts affect a small percentage of the total reprocessed data set, though they cause several week-long windows of missing data in the Amazon during some ERS orbits. It is also worth noting that the AMI sensor's scatterometer and SAR modes were mutually exclusive. Certain areas were frequently observed in SAR mode, significantly reducing the amount of scatterometer data available for that region.

As a note for clarity, the acronym ERS is used in this study to refer to the satellite program comprising ERS-1 and ERS-2, as well as the microwave sensor carried onboard, AMI. In some literature, the sensor is also known as ESCAT in keeping with the naming convention of several other sensors (NSCAT, ASCAT, and OSCAT), though this nomenclature is relatively uncommon compared to ERS.

4.2 ASCAT

Building on the experience gained from the ERS mission, the ESA developed an enhanced C-band sensor called the Advanced Scatterometer (ASCAT). To increase continuity with data collected from the previous C-band mission, the fundamental observational characteristics of ASCAT are similar to those of ERS. It operates at a frequency of 5.255 GHz and employs twin antennas, doubling its coverage area compared to ERS. Compared to ERS, ASCAT has exceptionally consistent coverage, fully measuring the Earth's surface every four days. The revisit period, meaning how much time passes between repeated measurements of a given location, is considerably lower due to ASCAT's increased swath area. And because ASCAT is a dedicated scatterometer sensor, there are no data blackouts from switching modes.

Advances in radar systems also permitted an increase in data resolution by using finer range gating to divide the antenna swath into slices. The incidence angle was also shifted to provide more useful data for ocean wind retrieval [21].

ASCAT was first launched aboard the *MetOp-A* satellite in 2006, followed by *MetOp-B* in 2012 and *MetOp-C* in 2018. Significant advancements were made in data transmission, ground station data capture, and instrument stability and calibration over its predecessor, providing researchers with more reliable data for use in geophysical modeling functions.

The success of ASCAT and other meteorological sensors aboard these satellites motivated a follow-on mission as a second generation of meteorological satellites called *MetOp-SG*. Satellites carrying an updated ASCAT sensor are planned to be launched in 2026. The sensor, called SCA, will provide data at increased resolution, additional VH polarization on mid-beam antennas, and increased swath width for improved global coverage [21].

5 Landscape Classification and Deforestation

5.1 C-Band Vegetation Dynamics

C-band sensors are often preferred over other microwave bands for vegetation studies due to their wavelength. This scale of interaction provides insight into both the soil and vegetation conditions in the measurement area. C-band radiation has more significant interaction with plant matter than L-band radiation but is not as heavily influenced by small-scale surface characteristics as Ku- or X-band, as illustrated in Figure 5.1.

The Amazon region receives significant attention in remote sensing literature, due in part to the regular cycles that it exhibits. The wet and dry seasons are one such cycle, yielding an identifiable annual variation in the backscatter signature. On a smaller timescale, daily precipitation occurs in a more or less regular cycle. Seasonal rainfall often occurs in the late afternoon and evening [23], which alters the distribution of water in the canopy. This causes notable variation between morning and evening passes from scatterometers, as C-band sensors show a particular sensitivity to vegetation water dynamics.

Certain regions within the Amazon experience minimal change month to month and even year to year. Due to a unique combination of vegetation and climate, microwave backscatter magnitude in these areas is so consistent that it can be used to calibrate spaceborne sensors like ASCAT and ERS, making them a well-established reference in Earth remote sensing [24]. Calibration is a necessary process in scatterometer studies as it protects against sensor drift over time and makes comparisons between different instruments possible by providing a reliable baseline for measurement. Without calibration, quantifying uncertainty would not be possible, preventing meaningful conclusions from being made based on ocean, soil, and vegetation backscatter values.

Generally, vegetation backscatter can be modeled as a combination of surface scattering (σ_s^0), canopy volume scattering (σ_c^0), soil scattering (σ_g^0), canopy-ground multiple path interactions (σ_{cg}^0), and multiple path ground-trunk interactions (σ_{gt}^0) [25]. Thus, total vegetation backscatter (σ_t^0) is expressed as:

$$\sigma^0 = \sigma_s^0 + \sigma_c^0 + \sigma_g^0 + \sigma_{cg}^0 + \sigma_{gt}^0 \tag{5.1}$$

The Amazon basin is composed of a range of ecosystems, spanning from dense forests to grasslands. Rainforests are a heterogeneous environment that is generally divided into four key layers: the topmost emergent layer comprised of the crowns of the tallest trees, the canopy which forms the thickest layer of vegetation, the understory layer consisting of shrubs and bushes, and the undergrowth layer of short plants and decaying organic matter. Savannas lack the upper layers present in the rainforest and instead are composed of tall grasses, bushes, and scattered stands of short trees.

A given land coverage type demonstrates distinct seasonal and daily variability, incidence angle dependence, and average brightness of its backscatter response [26]. For short land coverage types such as grasses, shrubs, and most agricultural crops, C-band backscatter is heavily influenced by the surface scattering of the underlying soil [27], primarily its

moisture content, while still exhibiting moderate sensitivity to vegetation characteristics. In dense forests like the Amazon, the backscatter response is dominated by volume scattering from the canopy and exhibits increased sensitivity to vegetation water dynamics. Drought, vegetation regrowth, and aging have significant impacts on the σ^0 brightness of heavily forested areas. In seasonal wetlands where regular flooding occurs, multiple scattering between the water's surface and vegetation can occur, altering both backscatter magnitude and incidence angle dependence [23].

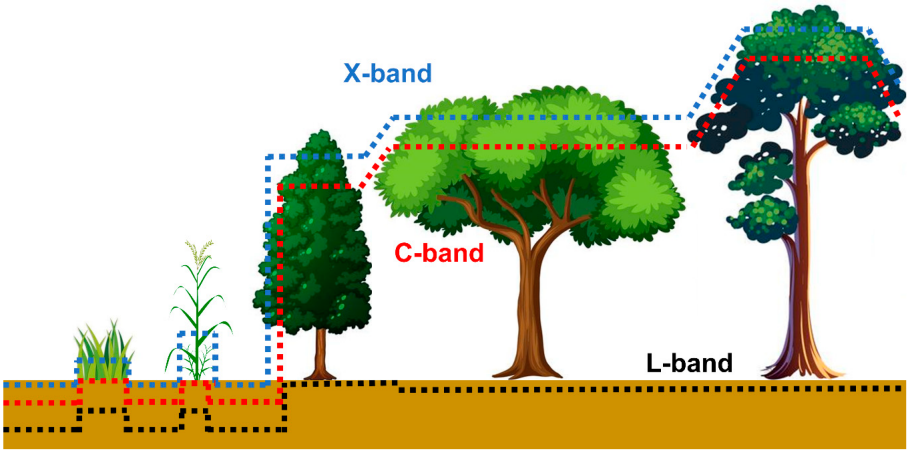

Figure 5.1: A demonstration of the penetration depth of different microwave bands in vegetation and soil. L-band (1-2 GHz) and low frequency radiation is generally able to penetrate vegetation and reach the soil. X-band (8-12 GHz) and higher-frequency microwave bands are unable to scatter off the upper layer of vegetation and are largely unable to reach the soil if it is covered by even short grasses. C-band radiation (4-8 GHz) is commonly used in vegetation studies because it penetrates short or sparse vegetation into the soil while scattering off tall, dense vegetation. This behavior creates an observable difference in C-band backscatter between vegetation types that can be used for classification. *Frappart, F., et. al. (2020). Global monitoring of the vegetation dynamics from the vegetation optical depth (VOD): A review. Remote Sensing, 12(18), 2915.*

Because the density and height of land coverage impacts the backscatter characteristics so significantly, a number of methods are used to classify the vegetation type present.

5.2 Landscape Classification

One approach to large-scale vegetation classification is to measure the "greenness" of a given area under optical imaging, known as a vegetation index. The most commonly used is the normalized difference vegetation index (NDVI). While the vegetation's greenness can indicate rainfall and overall health, NDVI does not directly relate to the vegetation water dynamics that C-band scatterometers are most sensitive to. For example, areas that appear similar to optical sensors can display distinct C-band backscatter behavior due to differing vegetation height and water distribution. Therefore, NDVI is not an adequate substitute for land coverage classification for the purposes of microwave scatterometer vegetation studies [27].

Rather than relying on optically-based vegetation indices, rough classification may be done based on C-band backscatter characteristics. By modeling the incidence angle dependence and vegetation cycles of different forms of land coverage, an area can be classified by vegetation type. It should be noted, however, that seasonal variation and soil moisture can reduce the accuracy of these models. Petchiappan observes that "an increase

in soil moisture results in an increase in vegetation backscatter at all incidence angles" [23]. A change in vegetation moisture changes incidence angle sensitivity. These factors acting in conjunction complicate classification efforts, especially if only a limited range of incidence angles is available. This interplay is described by Wagner for ERS (see Figure 5.2), demonstrating the difficulty of consistent classification. Incidence angle dependence varies throughout the year not only due to vegetation moisture but also due to seasonal cycles [26], such as death and regrowth, shedding leaves, and shifting biomass distribution in crops and seeding grasses.

In the Amazon and other tropical regions, seasonal flooding can dramatically influence the backscatter characteristics of vegetation. In non-flooded forests, the contribution of ground to trunk scattering is often negligible. However in flooded forests, the reflection off the water's surface can cause an increased contribution from surface and trunks, caused by significant multipath scattering off the standing water. The magnitude of this effect is dependent on frequency, polarization, and incidence angle. In HH-polarized C-band, the modeled impact of standing water is an increase of ≤2.0 dB, such that the volume scattering from the canopy remains the dominant scattering mechanism. The VV-polarized C-band backscatter, the kind of scatterometer measurement analyzed in this study, shows a less significant increase of ≤0.3 dB [25].

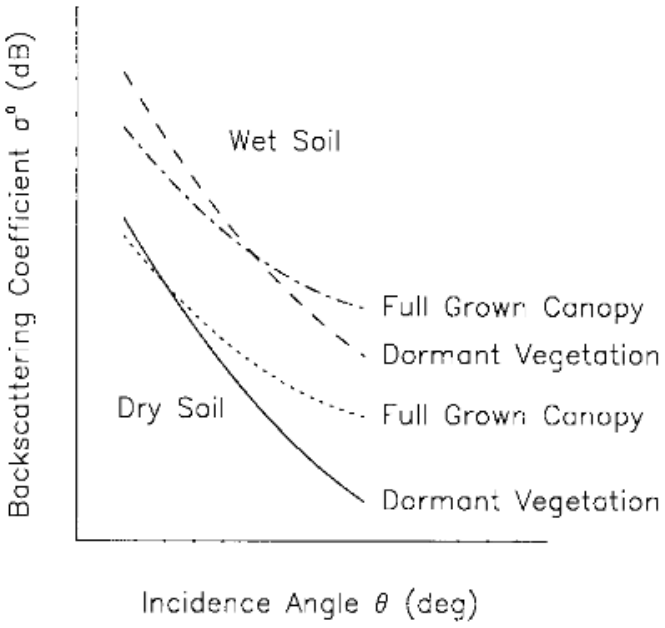

Figure 5.2: Generalization of vegetation backscatter magnitude in C-band at various incidence angles. At a particular incidence angle, the backscatter value for dormant and active vegetation crosses over, restricting the ability to classify vegetation density from individual measurements. Instead, multiple measurements over a single area are used to determine the incidence angle dependence of the backscatter, which characterizes the vegetation density. It is worth noting that soil moisture and canopy density are continuous values, causing further ambiguity in determining the state of vegetation. *Wagner, W., Lemoine, G., Borgeaud, M., & Rott, H. (1999). A study of vegetation cover effects on ERS scatterometer data. IEEE Transactions on Geoscience and Remote Sensing, 37(2), 938-948.*

Deforestation at the most basic level is a change in the type and amount of vegetation in a given area. Whereas the rainforest is typically characterized by tall, dense vegetation, deforestation results in limited remaining vegetation. Often, some small trees remain after deforestation occurs, but occasionally an area is cleared of all vegetation and low-lying shrubs and grasses reclaim the exposed area. The types of vegetation left behind after deforestation display backscatter characteristics that distinguish them from tropical vegetation, including higher incidence angle dependence, greater seasonal variability, and increased backscatter contribution from the ground [27]. This behavior permits discrimination between deforested areas and undisturbed vegetation in the scatterometer data.

5.3 Climate Zones

Another noteworthy approach to vegetation classification is done using climate zones. A common system, called the Köppen climate classification system, divides the world's surface into 5 classes and 30 subclasses based on their monthly air temperature and precipitation. These climate trends impact the type of vegetation that can grow in a given region, with relative consistency in vegetation between regions of the same classification.

Each climate zone is denoted by a two or three letter combination. The first letter corresponds to the broad climate group: A for tropical, B for dry, C for temperate, D for continental, and E for polar. The second letter represents the seasonal precipitation patterns, and the third represents the level of heat experienced through the year. The Köppen climate classification system is intended to represent the long-term mean of an area [28]. Therefore, while it is unlikely that the climate group (A-E) change in a given region, between years the precipitation characteristics might fluctuate enough to be classified differently. Even considering these interannual variations, it serves a widely-used analog for vegetation types in global climate studies and provides a succinct way to communicate land and climate trends [28].

A common view of the Amazon is that it is filled with dense jungles and consistent rain. In fact, it is composed of three zones with differing weather patterns and vegetation. True tropical rainforest climate zones (Af) experience rainfall year round with no dry season, though the amount of precipitation can differ significantly between months. Interestingly, plant growth in this interior region of the Amazon is limited by the amount of light it receives rather than by water like most other climates [23]. Tropical monsoon climate zones (Am) also receive large amounts of precipitation but have a distinct dry season. To be classified as a monsoon climate, a region must receive on average at least 60 mm of rain during its dry months. A region that receives less than 60 mm is classified as tropical savanna. The Amazonian savanna zone undergoes a dry season in the winter, so it is classified as dry winter savanna (Aw).

The savanna climate zone is of particular interest in this study because it is subject to the most severe degradation out of the three regions mentioned above. When forest is cleared by fires or agricultural use in the Amazon, scrub and grasses often repopulate the land and over several years, such large deforested areas can experience hotter and drier winters [29]. This phenomenon is often termed "savannization", though it may more accurately be described as human-derived savanna, and threatens large swaths of the Amazon rainforest.

Forest-replacing derived grassland should be distinguished from natural savannas, as they have distinct vegetation characteristics which significantly impact their ecosystems. Derived savannas are dominated by a small set of colonizing grasses which replace the

original tropical forest, leaving one or two dominant species. These areas can be more prone to wildfires, which can impact surrounding forests ill-adapted to fire [29].

Natural savannas are well-established and ecologically rich biomes that account for roughly 6% of the Legal Amazon [10]. Savanna biomes are typically covered in coarse grass with pockets of low trees, and are a distinct but important part of the Amazon ecosystem. Native savannas include the Chiquitania region of Colombia, the Lavrados de Roraima in northern Brazil, and Guianan savanna extending into the Brazilian states of Pará and Amapá. The Cerrado is another savanna ecosystem which lies partially within the Amazon River basin and encompasses much of the central region of Brazil [10]. These unique ecosystems suffer increased degradation due to a combination of less stringent environmental protections, ambiguity in classification, limited international recognition, and geographic accessibility for agricultural activity compared to dense interior forests. While discourse surrounding Amazon deforestation often focuses on the rainforest, tropical savannas are another vital part of the biosphere that deserve increased recognition and protection.

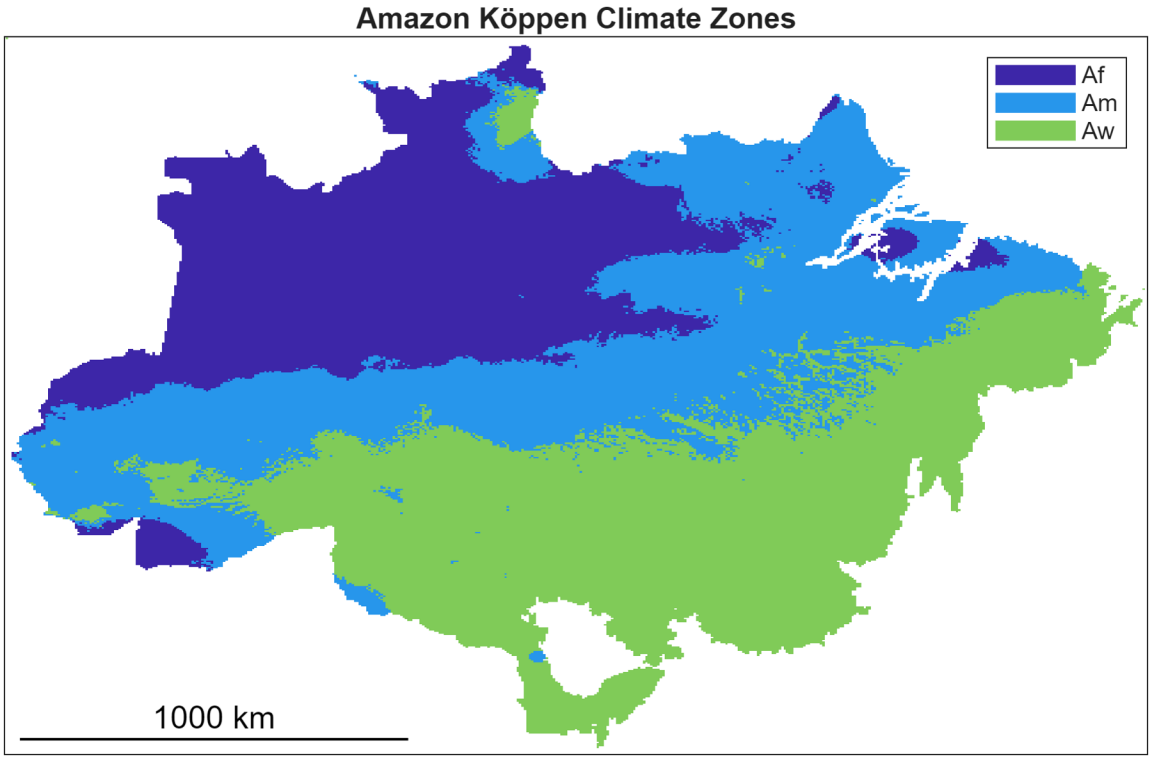

Figure 5.3: Köppen climate zones at 6.25 km resolution.

Thus, it is worth noting that the Köppen climate classification does not perfectly describe the kind of vegetation present. This applies within the tropical savanna climate as well as rainforest and monsoon climates present in the Amazon. Climate classification is useful for describing the general temperature and precipitation trends of a region and indicating what vegetation is likely to be found there, but certain areas might have unique land coverage that would seem counterintuitive if only their climate classification were considered.

6 Data Sources

6.1 Scatterometer Images

Scatterometers were conceived as an instrument for obtaining instantaneous localized wind speed estimates over the ocean, meaning that frequent global coverage was a high priority in the sensor design process [18]. Satellite instruments experience a tradeoff between resolution and coverage area, meaning one application may require a sensor covering a narrow swath at a high resolution while another benefits from a sensor with a wide swath width at a low resolution. In the end, ERS was designed with a nominal resolution of 50 km to match the desired grid size for ocean wind vector data. ASCAT has a nominal resolution of 25 km to fit more modern ocean wind vector products. Through the reprocessing done by the SCIRoCCo project [22], ERS data is also available at 25 km resolution. This 25 km resolution data is used for this paper, but it should be remembered that the coarse resolution of raw ERS measurements still impacts its usefulness for predicting fine spatial phenomena.

While this resolution is sufficient for ocean wind estimation, it is often too coarse for use in land or ice studies. Thus, image processing techniques have been created [30] that extend the usefulness of scatterometer data beyond ocean wind retrieval to a variety of other applications. One such technique is the scatterometer image reconstruction (SIR) algorithm developed by Brigham Young University's Microwave Earth Remote Sensing (MERS) lab. SIR-enhancement has been successfully applied to ERS [31] and ASCAT [32] for use in wind, ice, soil, and vegetation studies [33–35].

The SIR algorithm's performance depends upon sufficiently dense measurements, but is capable of significant improvements to sensor resolution. Enhanced resolution SIR images, sometimes called ultra-high resolution (UHR), are created by aggregating data from multiple passes over an area, normalizing the σ^0 measurements for incidence angle, and applying an iterative "drop-in-the-bucket" technique to assign measurements to a spatial grid [30, 36].

To create a UHR ERS image, for example, raw data is aggregated in either 6- or 18-day periods. Specific kinds of measurements may be selected for processing, such as data from ascending (north-bound) or descending (south-bound) passes of the instrument. The data then passes through 30 iterations of the SIR algorithm before the final data product is complete. The result is an image of σ^0 measurements across the world at a resolution of 6.25 km. These images are made publicly available for research use as 6- and 18-day scatterometer images [37].

In the realm of scatterometer image reconstruction, there is an innate interplay between spatial resolution, image time, and noise level [30]. Coarse-resolution data incorporates an inherent smoothing effect by averaging a large amount of data with random noise together [34]. On the other hand, the image reconstruction process tends to amplify high resolution noise [30]. Noise can be reduced by taking additional measurements of that subject, thus averaging more noisy data, but this requires a longer imaging time. For some applications like wind estimation, this is undesirable as a longer imaging window diminishes the ability

to make instantaneous measurements. Because deforestation is persistent and continues to impact the land long after the event occurs, long imaging windows are beneficial for the lower-noise data they provide. However, resolution is also an important factor, as too coarse a resolution would likely obscure the impact that deforestation has on backscatter response. With these constraints in mind, this study uses 18-day images from both ERS-1 and ERS-2 to minimize noise while maintaining as high a resolution as practical with the instrument.

ASCAT benefits from both a higher nominal resolution than ERS and greater swath area, thus ASCAT SIR images may be generated at a higher resolution or over shorter time periods. ASCAT data has been processed at a 3.125 km resolution, but lower-resolution data is used for consistency with the ERS images. The 6.25 km resolution ASCAT images used in this study are pulled from publicly available 4-day images, as they provide more consistent global coverage than 1- or 2-day images.

6.2 GIS Deforestation Data

The Brazilian government provides deforestation data in the form of Geographic Information Systems (GIS) shape files. This data contains the deforestation area and location, date recorded, and, in the case of DETER alerts, the cause of deforestation. PRODES and DETER deforestation data form the "ground truth" for developing and validating deforestation estimates based on the scatterometer data in the previous section.

As both datasets are based on optical images, deforestation area is reported with a much higher resolution than the scatterometer images. Thus, the deforestation shape files must be reprocessed to bring them to a resolution compatible with the UHR scatterometer images. This is accomplished by first generating a grid of pixel footprints corresponding to ASCAT or ERS measurements, calculating the percentage of overlap between each pixel and the deforestation polygons found therein, and exporting an image with the overlap area encoded in the pixel value. Each image is labeled with the date that the deforested area was first measured within the respective program, either PRODES or DETER. It is worth noting that these projects only measure deforestation within the Brazilian Amazon. Projects in other countries, such as Peru [38] and Colombia [39], are also maintained but are not considered for this study. Most deforestation events cover only a small fraction of a pixel's $\sim 40km^2$ area, meaning that it can take several months or years before a pixel is completely deforested. The vast majority of deforestation polygons in the database cover less than one percent of a pixel on a given date, but accumulate steadily over time. Thus, to track deforestation accurately it is important to provide a measurement of the total deforestation within an area over time, rather than individual events.

To accomplish this, PRODES and DETER deforestation images are combined to capture snapshots of deforestation each month. At the start of each year, the accumulated deforestation measured by PRODES is used as a baseline with DETER alert areas being added as they occur. At the end of the year, all deforestation measured by PRODES over the year is added to the previous years' PRODES deforestation image to establish a new baseline. This approach takes advantage of the timeliness of DETER alerts to capture deforestation as soon as possible after it has occurred, but also leverages the precision of PRODES data to minimize accumulated error in area and geographic distribution.

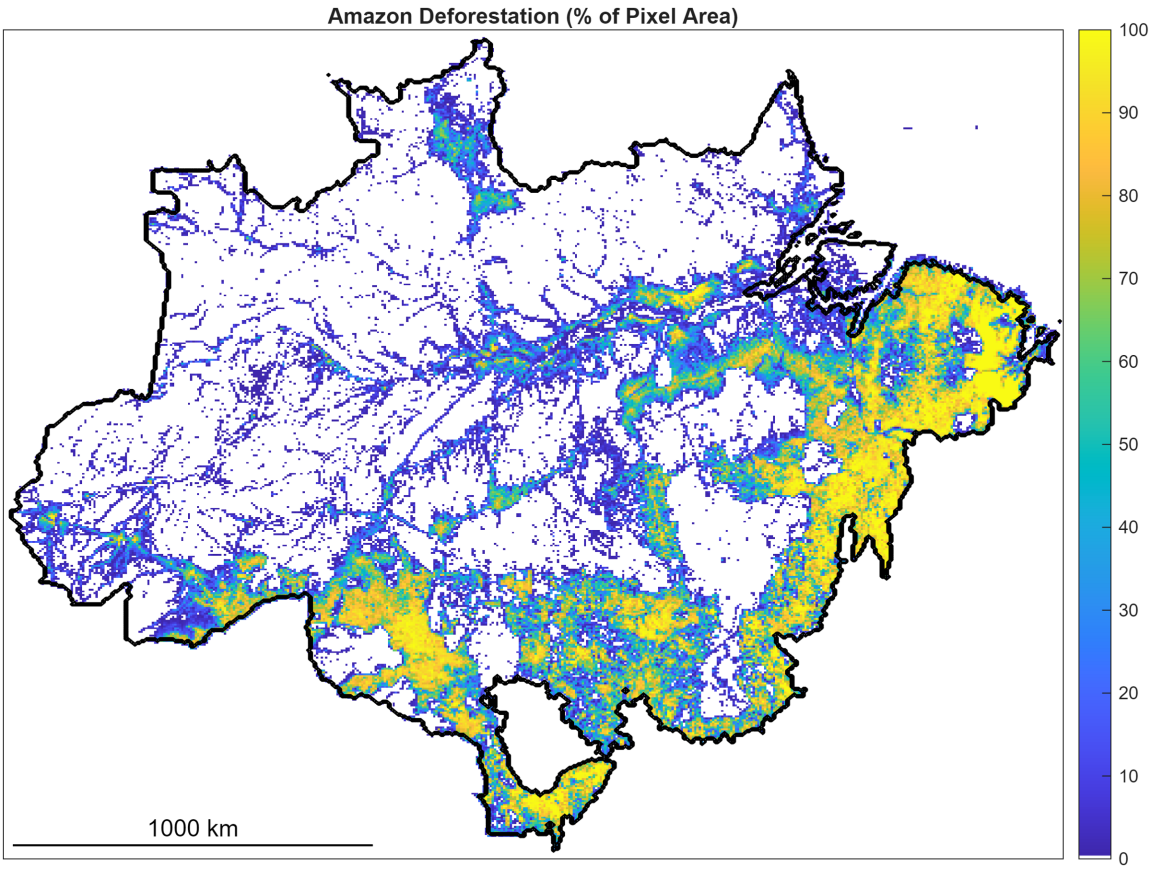

Figure 6.1: Per-pixel accumulated deforestation area of the Amazon for latest available data from PRODES and DETER, July 2023. Deforestation is especially concentrated along rivers and highway, as well as in the “arc of deforestation" in the southwest. This is where the majority of agriculture takes place, and thus the most intense landscape degradation. When validating deforestation predictions, a minimum area threshold is set and areas immediately surrounding water are masked.

6.3 Climate Classification and Landscape Coverage

To distinguish between the different vegetation types present throughout the Amazon, a climate classification map is used [40]. The original dataset provides a timeline of Köppen classification data at 1 km resolution, including projections into the future under different carbon emission scenarios [28]. Within the dataset, maps are available at 30-year intervals, meaning one map can encompass the operating lifespan of ASCAT or ERS. The 2004 map has been selected to best represent the climate conditions seen by both scatterometers. This map is down sampled to 6.25 km resolution using a nearest neighbor algorithm to match the UHR pixel grid of ASCAT and ERS.

High-resolution landscape classification data is also utilized in this research to determine water coverage. The MapBiomas project provides highly accurate land coverage maps, tracking human land-use, native vegetation type, and even the distribution of various crops within Brazil at 30 m resolution [41]. However, the aim of this research is to detect deforestation from microwave scatterometer data with minimal additional information. Therefore, only water coverage in the form of rivers, lakes, and reservoirs is considered.

As shown in Fig. 3.1, backscatter is heavily influenced by the roughness of the surface it is measuring. Water has both a high dielectric constant and a relatively smooth surface, such that the backscatter off of bodies of water is extremely low compared to *terra firma*. Thus, even a small body of water can significantly impact the σ^0 brightness of a pixel. Therefore, MapBiomas data is used to mask any pixel where a large enough area of water is present to appear in the dataset. Considering the resolution of the land coverage data is much higher than scatterometer data, masking all water is an extremely conservative approach to reducing σ^0 contamination, but preserves small lakes and tributaries that would otherwise disappear at coarse resolution.

All data is clipped to the Amazon biome as defined by the Brazilian National Institute for Space Research (INPE) [42], as this is the range in which PRODES and DETER deforestation alerts are provided. The boundaries defined by Amazon Network of Georeferenced Socio-Environmental Information (RAISG) are considered the extent of the Amazon, but only data within Brazil are considered. The RAISG Amazon borders also includes parts of Bolivia, Peru, and Venezuela, but these areas do not fall under PRODES and DETER deforestation monitoring.

7 Methodology

The data sources described above enable the comparison of deforestation and microwave backscatter response over time and provide necessary information for predicting deforestation within the three climate types present in the Amazon basin. The basis of the approach described herein is that by comparing a pixel's backscatter response to that of known undisturbed vegetation, the reduction in σ^0 brightness can be correlated linearly with the amount of deforestation present in that area.

7.1 Protected and Deforested Reference Zones

Areas of concentrated deforestation are also established, targeting regions of expanding development and agriculture. Again, two reference areas are selected for each climate zone. These areas show increasing human activity over the span of available PRODES and DETER alerts and exhibit varying concentrations of deforestation. Each deforestation region contains multiple cities and may include alerts related to agriculture, fires, urban expansion, road development, mining, and logging. The following cities and their surroundings are targeted:

Ref. Zone	City	State	Climate	Avg Temp. (°C)	Avg Rainfall (mm)
1	Colíder	MT	Aw	26.7	2011
2	Santana do Araguaia	PA	Aw	27.0	1807
3	Rio Branco	AC	Am	25.6	1692
4	Altamira	PA	Am	26.8	2008
5	Rorainópolis	RR	Af	27.5	2126
6	Ipixuna	AM	Af	25.8	2504

Table 7.1: Deforestation study areas. Two are selected for each climate zone, targeting areas of concentrated deforestation with protected landscapes nearby. *Fick, S. E., & Hijmans, R. J. (2017). WorldClim 2: new 1-km spatial resolution climate surfaces for global land areas. International journal of climatology, 37(12), 4302-4315.*

In order to isolate the impact of deforestation on backscatter, areas of known deforestation are compared to undisturbed vegetation in nearby ecologically protected areas. Two reference areas with minimal deforestation are established in each climate zone. Reference areas contain minimal deforestation alerts over a large contiguous area for the duration of available DETER and PRODES data and are chosen to target official designated indigenous territories, national forests, and ecological reserves. Because of the coarse resolution of microwave data, it is neither practical nor beneficial to closely follow the boundaries of these protected areas too closely when extracting deforestation and σ^0 data. Instead, rectangular areas are selected that sit well within the protected zone.

Protected areas are chosen to be in proximity to a particular deforested study area and are numbered accordingly:

1. Menkragnoti Indigenous Territory, Pará (Aw climate)
2. Kayapó Indigenous Territory, Pará (Aw climate)
3. Camicuã Indigenous Territory, Amazonas and Mapiá-Inauini National Forest, Amazonas (Am climate)
4. Araweté/Igarapé Ipixuna Indigenous Territory, Pará and Terra do Meio Ecological Station, Pará (Am climate)
5. Rio Trombetas Biological Reserve, Pará and Uatumã Biological Reserve, Amazonas (Af climate)
6. Vale do Jaravi Indigenous Reserve, Amazonas (Af climate)

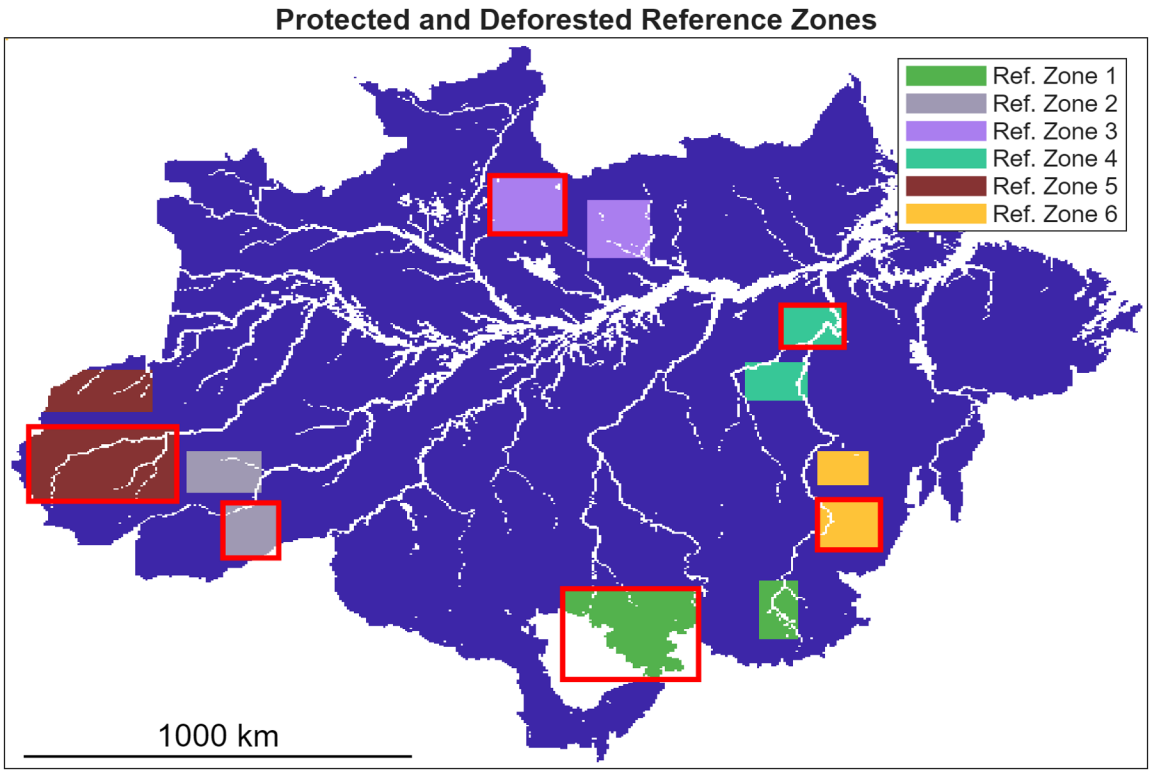

Figure 7.1: Deforested study areas are shown outlined in red. Deforested areas are chosen for their high density of deforestation and varied patterns of land use. Protected areas are selected to be in the middle of ecological or indigenous preserves that have experienced minimal deforestation. They are situated as close as possible to the associated deforested area in order to reduce variance in climate and vegetation.

For the sake of brevity, deforested and protected areas are referenced together using their shared zone number, as the deforested and protected areas are being compared to one another. For example, "reference zone #1" refers to both the protected study area within the Menkragnoti Indigenous and the study area surrounding the city of Colíder, Mato Grosso. When distinction is necessary, the protected or deforested area are specified as protected zone #1 and deforested zone #1.

Protected zones provide a baseline for backscatter measurements of undisturbed vegetation in a given climate zone and geographical area. A monthly average σ^0 is recorded

over each protected zone, omitting pixels where any deforestation has occurred (> 0.1% of pixel area) or where bodies of water are present. As the protected study region is largely undisturbed, changes in the mean σ^0 over time are considered to be the result of natural seasonal vegetation cycles and regional precipitation. Individual monthly σ^0 measurements are also accumulated over the span of available data to establish nominal backscatter variance for non-deforested landscapes within each zone.

The monthly mean σ^0 value from the protected zone is used to calculate backscatter anomaly values in the corresponding deforested zone by subtracting the monthly mean from each individual pixel's σ^0 value for that month. The pixel's backscatter anomaly is paired with the accumulated deforestation area recorded that month. Deforestation-anomaly data pairs are accumulated, omitting pixels where a negligible amount of deforestation has occurred (< 0.1% of pixel area) or where bodies of water are present.

Two forms of linear regression are applied to the deforestation-anomaly data in each zone. The first approach finds the mean of anomaly values at each percentage value of deforestation, which forms the input to a simple linear regression. The second approach selects the most common anomaly value at each deforestation percentage for use in a linear regression, a technique sometimes known as "peak picking" or "max pooling". This is done to explore whether one approach is more representative or robust to noise in the backscatter data.

Finally, these regressions are applied to the backscatter anomaly data within the study region to predict deforestation values. The deforestation predictions are compared to accumulated deforestation data, measuring both the total predicted deforestation area and two-dimensional cross-correlation between predicted and measured deforestation. Pixels with an anomaly value below the noise threshold of one standard deviation for non-deforested backscatter measurements are not considered. Pixels for which the *in situ* deforestation area is lower than the equivalent required σ^0 anomaly value in the regression are not considered. An accurate regression produces a prediction with high spatial correlation (close to 1) and a total predicted deforested area close to the sum of accumulated deforestation at that time.

7.2 Climate Zone Prediction

Beyond the reference areas, regressions are applied to all backscatter measurements for a given month within a climate zone. With the regression coefficients calculated for each reference zone, predictions are made for deforestation within each climate zone and compared to ground truth deforestation data. These predictions are evaluated using the same criteria of cross-correlation and total predicted deforestation area as described above.

By applying the regression derived from each reference zone to σ^0 anomalies across its respective climate zone, it is possible to quantify well the reference area represents vegetation in its climate. The same metrics of accuracy previously mentioned, total area and 2-D cross-correlation, apply when predicting deforestation for a climate zone. This also allows reference areas in the same climate zone to be compared to each other to determine which most accurately predicts deforestation.

This approach, however, relies on a few key assumptions. A primary assumption made is that vegetation and weather patterns within a climate zone are reasonably similar, even when spread over a large geographical area. By applying the same regression parameters to a whole climate zone, it is assumed that each location experiences comparable temperatures, sunlight, and rainfall regardless of location. Consistency within a climate zone is implied

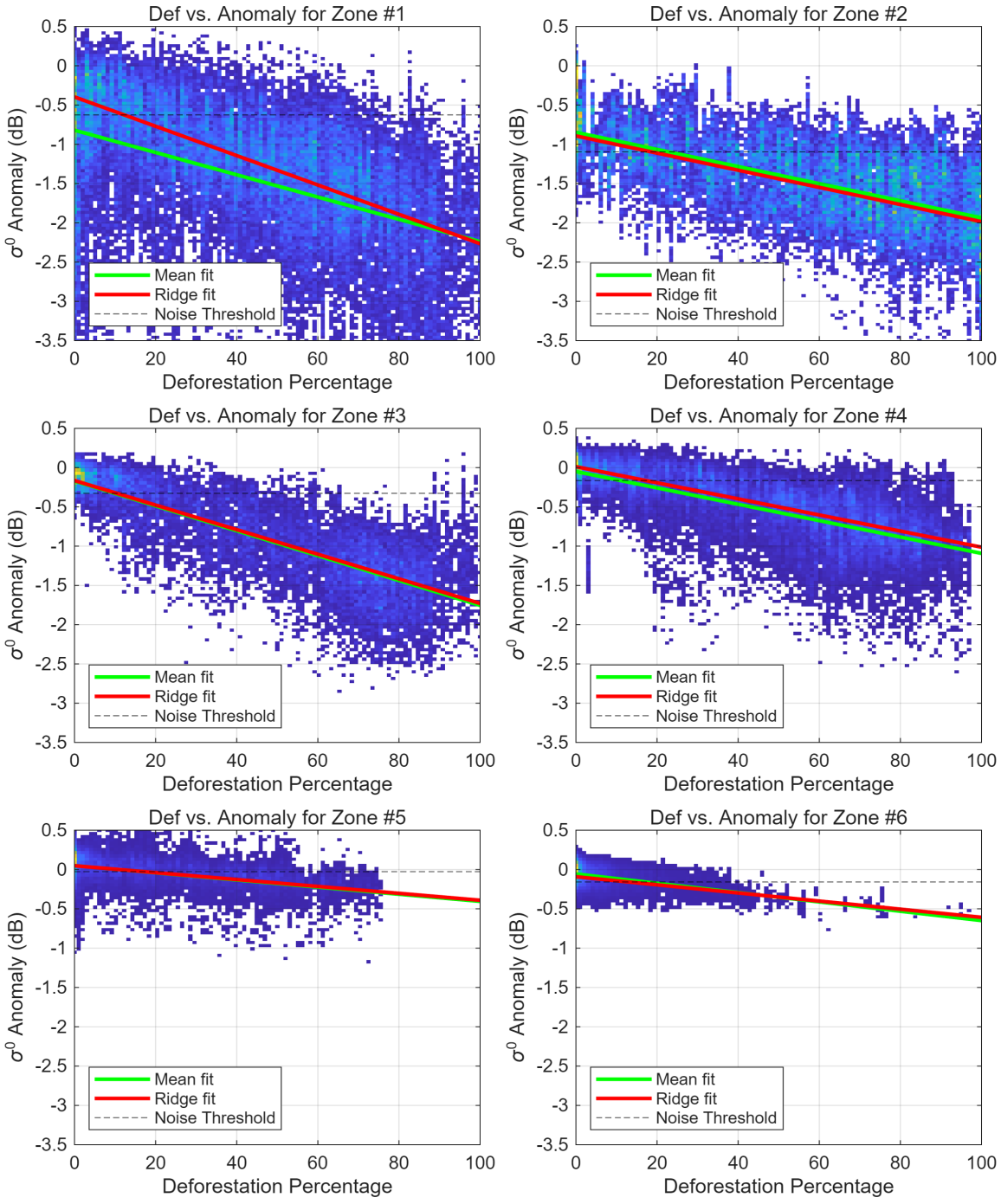

Figure 7.2: Linear regressions using "peak" and "mean" techniques. Each of the six reference zones is shown, paired by climate zone. Note that reference zones #5 and #6 both have noticeably shallower slopes than other regressions, meaning there is less difference in backscatter between deforested and non-deforested pixels.

to a certain extent by classifying locations together in the classification system, but there may still be significant variation that falls within a single climate zone's parameters. Similarly, by applying a regression to the entirety of a climate zone, it is assumed that different species of vegetation within a zone share similar backscatter characteristics and

are impacted by deforestation in comparable ways. Both are fairly standard assumptions made in scatterometer research involving vegetation [23][27] and climate patterns [43] and acknowledged within the literature.

An additional assumption is that there is a clear separation between different climate zones, both in land coverage and backscatter behavior. In other words, by classifying the landscape using solely the Köppen climate system, areas within different climate zones can not be effectively compared to one another even when situated in proximity to one another. In reality, there are areas of transition for both climate patterns and vegetation. The assumption that climate zone is the dominant factor in the backscatter response of deforested land arises from the purposefully limited data used for classification. For the most part, grassland transitions to forest and rainfall increases only gradually as one approaches the center of the Amazon Basin. While a highly granular map of vegetation types, such as MapBiomas, would allow for more accurate grouping, the aim of this study is to rely primarily on microwave imaging and include as little additional information as possible about the landscape. By minimizing the amount of prior knowledge required to detect deforestation, the predictive framework can be more readily applied to tropical forests beyond the Amazon.

7.3 Deforestation Detection

Beyond estimating deforestation area in a pixel, the viability of microwave scatterometer data as a detector of deforestation is also evaluated. A detector is a statistical tool for testing hypotheses [44], often denoted as H_0 (hypothesis zero or the null hypothesis), hypothesis H_1, hypothesis H_2, etc. Binary detectors provide a simple way of determining whether one state is more likely than another considering a set of observations, such as if a pixel is deforested (H_0) or not (H_1) based on microwave backscatter data.

A threshold detector compares the estimated deforestation level (x), as predicted by the mean linear regression defined above, to a determined minimum deforestation percentage (δ), such that [45]:

$$\phi(x) = \begin{cases} 0 \sim H_0, & x < \delta \\ 1 \sim H_1, & x \geq \delta \end{cases} \tag{7.1}$$

In order to determine the accuracy of the detector, the ground truth data must also be thresholded for comparison. The ground truth data is processed such that only pixels with a deforestation area above the noise floor (one standard deviation for non-deforested backscatter σ^0 measurements, see Fig. *something*) are designated as deforested. The detector is applied to the study area's predicted deforestation and compared to the true distribution of deforestation.

Detector accuracy is determined by two metrics: hit rate and false positive rate. Hit rate (α) is defined as the percentage of deforested pixels (DP) that the detector accurately identifies (TP)

$$\alpha(\delta) = \frac{TP}{DP} \tag{7.2}$$

The false positive rate describes how frequently the detector misidentifies pixels as deforested,

$$\beta(\delta) = \frac{FP}{FP + TN} \tag{7.3}$$

where β is the false positive rate, FP is the number of false positives, and TN is the number of true non-deforested pixels (true negatives). To be accurate, a detector must have a high hit rate while not misidentifying too many pixels. For example, a detector might accurately identify all deforested pixels, but have an extremely high false positive rate because it marks every single pixel as deforested. Thus, both measurements are required to understand a detector's performance.

The detector can be characterized by sweeping the minimum predicted deforestation percentage needed for detection and recording the hit rate and false alarm rate at that threshold. The receiver operating characteristic, such as the one shown in Figure 8.8, plots these values to visualize the tradeoff between hit rate and false positive rate. The formula for determining the optimum deforestation detector for an area is defined as

$$\delta_{opt} = \arg \min_{\delta \in [0,100]} \sqrt{\beta(\delta)^2 + (1 - \alpha(\delta))^2} \tag{7.4}$$

which represents the point closest to the upper left hand corner of the ROC plot for that study region. Detectors are created for both the deforestation reference areas and each climate zone and serve as an alternative method to estimation for predicting deforestation from microwave backscatter data.

A detector is established by first taking the measured deforestation in a reference zone or climate and threshold deforestation values to a minimum detectable amount, meaning that pixels with deforestation below that amount are set to 0 and pixels above are set to 1. Then, a "mean" regression is used to generate a deforestation prediction and classified using a swept deforestation threshold. An optimal detection percentage is identified using Equation 7.4 and the detector's performance is characterized using this value. The detection rate ($\alpha(\delta)$), false positive rate ($\beta(\delta)$), spatial correlation, and distance from a perfect detector are used to evaluate detector performance.

8 Results

By applying this methodology to ASCAT backscatter data, accurate predictions can be made for a wide variety of landscapes (see Table 8.1 for metrics for each reference zone). Multiple factors impact predictive performance positively and negatively including deforestation density, hydrology, ecology, climatic variation, and feature size.

For all of the predictions, a "peak" regression is applied to ASCAT data from the Amazon's dry season to achieve the best results. Strong correlation is found between predicted and measured deforestation in at least one reference zone in each climate (see Table 7.1), showing the regression to be especially capable of reconstructing vegetation patterns surrounding urban development and within protected areas.

When regressions are applied to a wider climate zone, the impact of confounding factors multiplies, limiting this approach's usefulness for large-scale prediction. However, for certain climate zones, the predictive regressions perform with high enough accuracy to meaningfully indicate deforestation patterns. General patterns of land use can be established using this approach.

The ERS scatterometer's effectiveness for predicting deforestation is compared to the ASCAT sensor. Differences in calibration, coverage area, and mission aims are discussed, including their impact on vegetation studies within this study.

Finally, detector performance is also considered and possible applications are discussed. While this methodology is not targeted at deforestation, meaningful conclusions about environmental policy enforcement can be drawn from the results. Detector techniques are best applied at a smaller scale, such as within reference zones, but can highlight areas of interest when applied to large biomes in climate zones.

8.1 Reference Zone Prediction

Ref. Zone	Min. Def. (%)	Total Def.	Peak Def.	Peak Corr.	Mean Def.	Mean Corr.
1	11.5	79,270	97,208	0.738	80,604	0.681
2	16.3	37,247	32,758	0.739	36,843	0.765
3	8.9	33,573	32,976	0.861	31,376	0.857
4	13.2	28,115	30,635	0.608	29,550	0.598
5	15.4	10,169	14,451	0.258	20,641	0.329
6	8.7	16,227	17,447	0.756	19,652	0.752

Table 8.1: Reference zone prediction accuracy for July 2023. "Peak" refers to a linear regression created using the most common σ^0 anomaly per deforestation percentage, as described in Section 7.1, while "Mean" refers to regressions using a true mean. In general, peak regression-based predictions show slightly higher spatial correlation to *in situ* data, though results are generally comparable between the two methods. Correlation coefficients above 0.7 are considered a strong correlation between deforestation and backscatter anomaly.

Within the tropical savanna climate, a strong differentiation between protected and deforested area aids in the accuracy of prediction. The region in which reference zones #1 and #2 are located has been subject to significant savannization, resulting in mean backscatter values for deforested pixels that are 1.5-2 dB lower than non-deforested pixels. Surrounding both reference zones' primary cities, Colíder, Mato Grosso and Santana do Araguaia, Pará respectively, deforestation is evenly distributed. Additionally, in these study areas the individual pixel values for deforestation area are high, strongly differentiating their backscatter measurements from non-deforested pixels. Both attributes contribute to prediction accuracy. These regions perform very similarly, likely due to their geographic proximity and shared vegetation types. While predictions tend to max out around cities, numerous regions of low deforestation are accurately reconstructed within both reference zones, even some that are only 2-4 pixels across (see Figure A.1).

Predictions in reference zone #3, surrounding Rio Branco, Acre exhibit the best metrics out of all of the areas studied, with a prediction correlation of 0.86 and area estimates that are accurate within 1.78% for the "peak" regression (see Table 8.1). The lack of major bodies of water enable accurate prediction of both area and spatial distribution, as well as a sharp backscatter drop off with deforestation (see Figure 7.2). Distinct hot spots are clearly visible around each of the cities and gaps between cities are preserved.

While also situated in the tropical monsoon climate zone, reference zone #4, centered on Altamira, Pará, does not perform quite as well as the previous area, with slightly less accurate area estimates and a correlation of 0.60. Altamira and its neighboring cities lie along the Xingu River, a major tributary of the Amazon. As established previously, bodies of water have significantly lower backscatter than land and, with coarse resolution sensors like ASCAT, can lower the measured brightness of surrounding land. The model has difficulty resolving landscape degradation from farmlands extending from the Trans-Amazonian highway in the area and predicts highly concentrated deforestation immediately surrounding the river. This effect, however, is significantly reduced when using scatterometer measurements from the dry season, as opposed to the wet season.

The region with the least accurate prediction is found within the tropical rainforest climate (Af) surrounding Rorainópolis, Roraima. Backscatter values for the few highly deforested pixels present differ on average by only -0.5 dB from non-deforested land. The poor differentiation in deforested and non-deforested backscatter response may be a product of the kind of vegetation present in this region or a protected zone that does not adequately represent the vegetation found within the deforested study area. These effects ultimately lead to low spatial correlation and a significant overestimate in deforestation area within this region.

Interestingly, the northwest of this region is sparsely vegetated, but does not any have associated alerts included in PRODES or DETER deforestation data. This area is part of Viruá National Park, an alluvial fan home to sandy forests known as *campinaranas* [46]. Despite having no value for agriculture or grazing due to its highly acid, nutrient-poor soil, it is one of the most biodiverse areas of Brazil and is estimated to house more than 5,000 species of plants [8].

This serves as an example of a consequence of methodological choices: the assumption of homogeneity within a climate zone. Viruá National Park lies within the tropical rainforest climate, but due to local geological and hydrological conditions is home to a distinct class of vegetation from the immediate surroundings. Because this methodology compares vegetation density to a determined reference area, any less-dense vegetation type is marked as deforested even when perfectly undisturbed such as in this case. Thus, an understanding

of native vegetation in the study area is beneficial for accurately distinguishing between human-driven landscape degradation from natural variation, even within a relatively small area. Other noteworthy factors in prediction accuracy are deforestation feature scale and

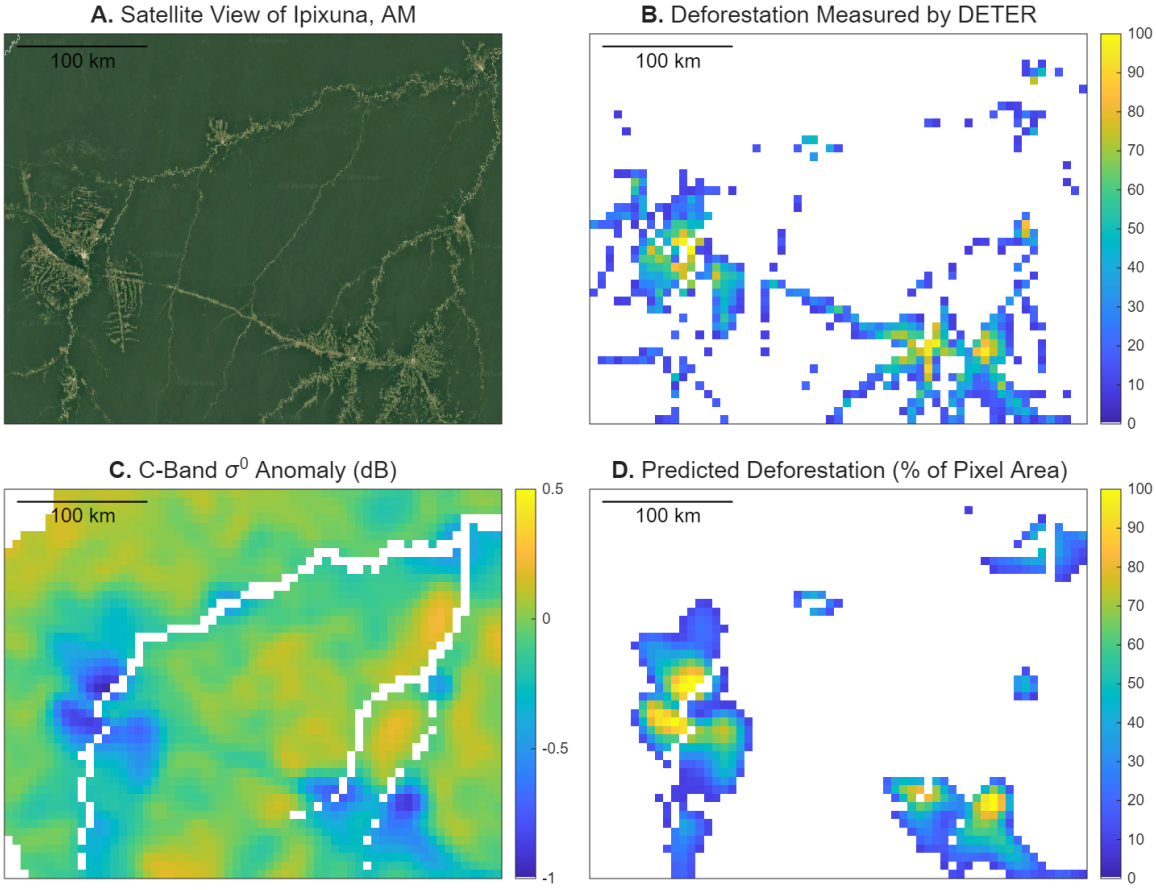

Figure 8.1: Deforestation prediction for July 2023 in Reference Zone #6, which estimates deforested area within 7.5% using the peak selection regression, as described in section 7.1. The deforestation data used for comparison is thresholded to the minimum detectable amount in this region. While this prediction is not the best-performing out of the areas considered, it clearly depicts the strengths and weaknesses of the methodology developed. The non-deforested strip between the two cities on the left-hand side of the image has a noticeable impact on the prediction in **D.**, demonstrating how fine features are smoothed but large areas of deforestation are retained. Neither the road extending northwest out of the cluster of cities on the lower right of **A.** nor the river just to the south of the road are captured by the predictor.

variation within climate zones. The model's performance in reference zone #6 demonstrates both of these effects. Firstly, Ipixuna, Amazonas, is located within the same climate zone as Rorainópolis but experiences greater rainfall and lower average temperatures over the course of the year (see Table 7.1. The differences in climate and other local conditions result in vegetation patterns that are more easily distinguished using the methodology developed above. Small-scale deforestation features along roads and immediately surrounding rivers are generally lost due to the coarse resolution of the ASCAT sensor. Figure 8.1 illustrates the effect of feature scale on prediction accuracy. The high-resolution comparisons of *in situ* data and predictions found in Appendix A may be consulted to see the results in greater detail. See Figure A.7 for an overlaid comparison of deforestation and predictions of each reference zone.

Because of the coarse resolution of the ASCAT sensor, predictions within reference zones effectively create a smoothed reconstruction of *in situ* deforestation data. The locations of concentrated pockets of deforestation and protected vegetation are accurately predicted, especially surrounding urban development.

While these factors can negatively impact performance, they are significantly offset by the strengths of the methodology. Predictions are most accurate when analyzing dense pockets of deforestation at a large scale, but the model can produce clear and useful results in a wide range of conditions. The limitations delineated previously illustrate how deliberate methodological choices impact model accuracy and demonstrate the robust performance of this reconstruction process.

8.2 Climate Zone Prediction

The strengths and the limitations developed in the previous section apply directly to deforestation predictions for the climate zones. The impact of hydrological, climatic, and biological factors is made more apparent with the wider geographical area. In this section, general trends and a few areas of interest are highlighted. Particular emphasis is given to protected conservation areas throughout the Amazon and how the selection of reference areas affects prediction within a climate zone.

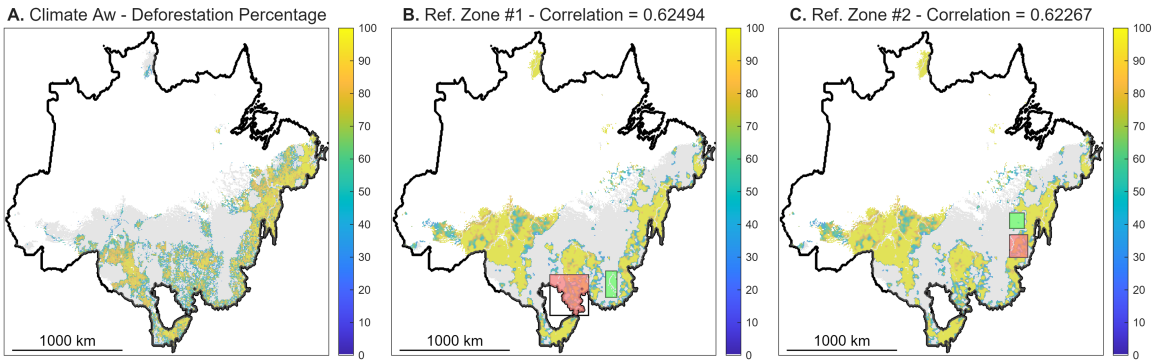

Figure 8.2: Deforestation area predictions for the tropical winter savanna (Aw) climate zone compared to *in situ* deforestation data as of July 2023. The reference zone used for each prediction is shown with the deforested area in red and the protected area in green. The deforestation data and ASCAT enhanced-resolution backscatter used for prediction date July, 2023. Larger images of deforestation distribution and all predictions can be found in Appendix B.

As with reference zones, predictions within the tropical winter savanna climate are generally more accurate than other climate zones. Because reference zones #1 and #2 are so similar in terms of climate (Table 7.1) and vegetation, regressions from these deforestation areas produced near-identical predictions. Strong correlation coefficients of 0.754 and 0.755 are achieved, which is similar to the reference zones' statistics, but area is dramatically overestimated. These predictions replicate the boundaries of protected landscapes with a high degree of accuracy in the south and east, preserving their protected reference areas and areas of similar vegetation very clearly.

However, the northeast and far west of the Aw climate zone both stand out in the predictions. The northeast shows anomalously low deforestation predictions where *in situ* data shows it to be widespread and highly concentrated. This suggests that the vegetation in this coastal northeastern region is more dense than that of the protected reference

Ref.	Climate	Total Def.	Peak Def.	Peak Corr.	Mean Def.	Mean Corr.
1	Aw	1,385,995	2,432,058	0.754	2,172,360	0.765
2	Aw	1,385,995	2,452,989	0.755	2,414,787	0.759
3	Am	426,776	399,868	0.508	375,405	0.508
4	Am	426,776	509,153	0.510	376,101	0.509
5	Af	63,088	266,052	0.219	247,408	0.212
6	Af	63,088	742,431	0.190	760,396	0.190

Table 8.2: Climate zone prediction accuracy for July 2023. Areas are measured in pixels.

areas further south, even when impacted by human activity. On the other hand, high levels of deforestation are predicted in the west where there is virtually none. It may be that vegetation in this region behaves in a manner more radiometrically similar to the tropical monsoon climate, rendering comparison to native savanna vegetation backscatter unproductive.

Deforestation predictions in the tropical monsoon climate show very similar trends, despite the reference areas being geographically separated. These predictions generally overestimate deforestation along major waterways, but attain reasonable accuracy around the southwest and eastern-central Amazon where the two reference areas are located. As noted in the analysis of deforestation surrounding Rorainópolis, RR (reference zone #5), naturally-occurring grasslands are shown as probable areas of deforestation, highlighting the distinction between climate zone and ecosystem classification. The same principles of local climatic and ecological variation apply as well to the central Amazon region, where widespread deforestation is inaccurately predicted at low levels. The resulting predictions apply well to areas most climatically similar or geographically proximate to the reference zones, but do not accurately describe areas that are farther removed. A correlation coefficient of 0.510 is achieved for reference zone #4 and similar for zone #3, though if predictions area were reduced, significantly higher correlation could be achieved.

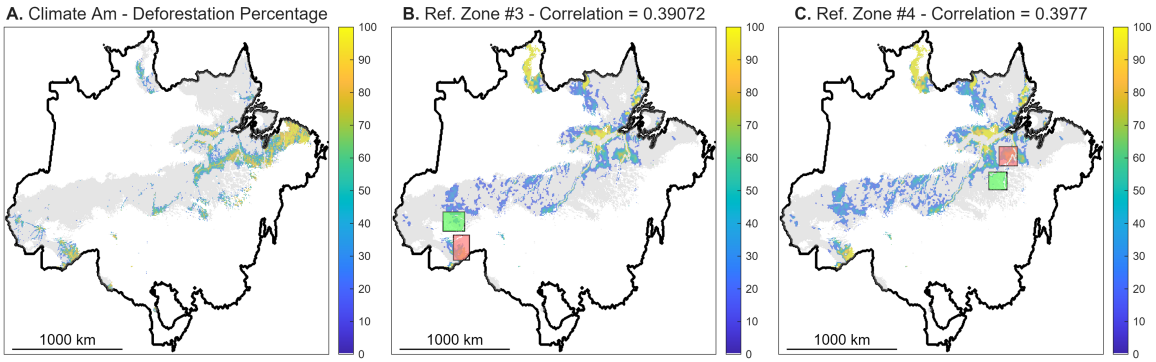

Figure 8.3: Deforestation area predictions for the tropical monsoon (Am) climate zone compared to *in situ* deforestation data as of July 2023. The two northernmost areas where concentrated deforestation is predicted correspond with the Lavrados de Roraima in the northwest and Guianan savanna in the northeast, two tropical grassland ecosystems within the Amazon

As a result of its remoteness, deforestation is not widespread in the tropical rainforest climate, making the Af region more difficult to validate than other climate zones. Major concentrations of landscape degradation can be observed surrounding Rorainópolis, Roraima (reference zone #5) and the city of Manaus, Amazonas. Manaus is located on the banks of Amazon River at its convergence with the Rio Negro, and as such the backscatter response of the surrounding area is dominated by the waterways. The distribution of deforestation/σ^0 anomaly data pairs show little to no correlation between the two variables, rendering Manaus and its surroundings nonviable as a reference area for the rest of the Amazon rainforest.

Thus, to provide a second reference for the climate zone, Ipixuna, Amazonas (reference zone #6) is still considered despite its deforestation area lying outside the limits of the climate zone. Reference zone #6 serves to demonstrate the limitations of applying a regression created in one region to predict vegetation suppression in another region. The regression based on the area surrounding Ipixuna noticeably overestimates deforestation area, suggesting that backscatter for undisturbed vegetation in the tropical rainforest climate zone (Af) can be significantly lower than in the tropical monsoon climate (Am).

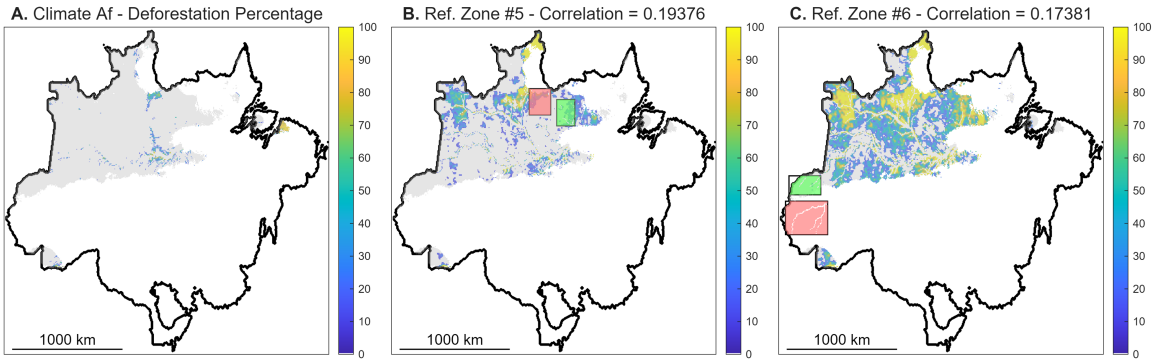

Figure 8.4: Deforestation area predictions for the tropical rainforest (Af) climate zone compared to *in situ* deforestation data as of July 2023. Note that the deforestation area for reference zone #6, Ipixuna, Amazonas, lies outside the Af climate zone while the protected area lies within the climate zone.

Both tropical rainforest predictions demonstrate hot spots corresponding to ecosystems with low vegetation density, much like Viruá National Park found within reference zone #5 in Section 8.1. One such is the Alto do Rio Negro Indigenous Territory found in the far northwest of the Amazon, which is composed of *campinaranas* interspersed with rainforest. This again highlights that climate zones contain many ecosystems with differing vegetation densities. Because this methodology compares a pixel's vegetation density to a reference area *vis-à-vis* backscatter magnitude, naturally occurring regions of low vegetation density are classified alongside areas suffering anthropogenic landscape degradation as being deforested.

In general, predictions from a reference zone are also applicable to regions that have similar vegetation and climatic conditions. Thus, deforestation in areas surrounding the reference zone tends to be reconstructed the most accurately, while deforestation in more remote areas may be significantly over- or underestimated. The predictions generated for wider climate zones are useful for showing areas of concentrated deforestation or regions that are generally undisturbed, but may be limited in their accuracy by a range of environmental factors.

The problem of regional variation can be counteracted either by limiting the range over which the regression is applied or by selecting representative reference areas for particular regions. In the case of the tropical monsoon climate zone (see Am predictions in Figure 8.3), the predictions close to Rio Branco, Acre and Altamira, Pará (deforestation areas #3 and #4 respectively) follow measured deforestation data exceptionally well. Major pockets of deforestation are accurately identified in the presence of large bodies of water, such as on the north bank of the Amazon river. The deforestation following the Trans-Amazonian highway on which Altamira is located (starting just to the east of deforestation zone #4 and continuing southwest) can also be seen in both predictions. Therefore, rather than by extending to an entire climate region, robust results can be obtained by extending beyond carefully selected reference areas.

8.3 ERS Performance

As discussed previously, the European Space Agency has operated two sets of C-band satellite scatterometer missions with similar measurement characteristics: ERS and ASCAT. Analysis up to this point has been focused on the latter, but deliberate attention should also be given to ERS. The two missions shared similar frequencies, incidence angle ranges, measurement footprints, and orbits, differing primarily in swath area [21]. Thus, it is natural to consider both sensors to extend the window of time covered by the data.

However, ERS differs in a few key regards that significantly impact its utility for predicting deforestation. Chief among them are their resolution and spatial coverage. In Figure 8.5, σ^0 data over the same time period from the two sensors is placed side by side for comparison. Due to its higher base resolution, spatial details in the ASCAT image are much more apparent. In the ERS image, backscatter appears similar the monsoon and savanna climate zones, whereas ASCAT shows a clear delineation between these climates.

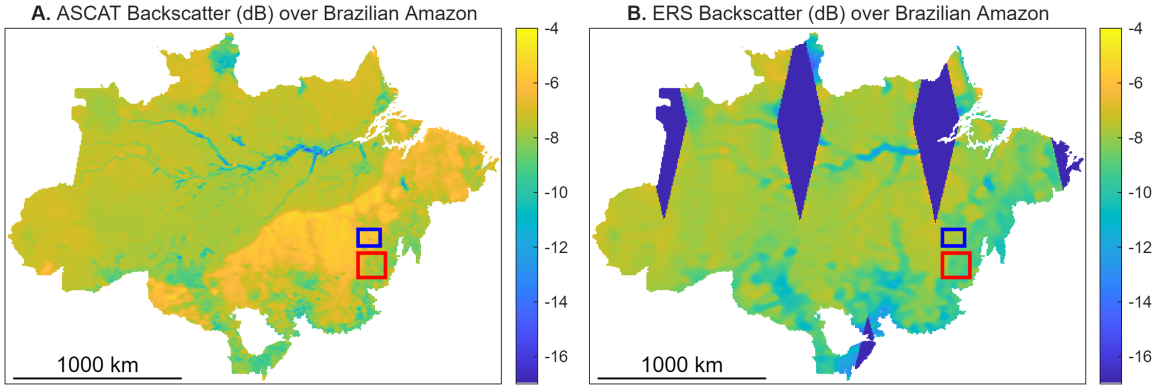

Figure 8.5: C-band backscatter measurements normalized to 40° incidence angle, taken June 2011, showing ASCAT UHR data on the left and enhanced resolution ERS data on the right. Reference zone #2 is highlighted in both images, with a red box containing the deforestation study area and a blue box containing the protected study area. Dark blue regions in the ERS scatterometer image denote areas within the Amazon where no data is captured. Both images show scatterometer data averaged over a one-month period, taken in 4-day windows in the case of ASCAT and 16-day windows in the case of ERS.

Large windows of missing data are also apparent in the ERS image. Particularly centered at the equator, large areas may not be measured in a one month period due to the sensor's smaller swath compared to ASCAT. Approximately 87% of the Amazon is covered by the ERS sensor in Figure 8.5-B, but for large periods of ERS-2's operating lifetime, scatterometer

data is available for less than half (or even none) of the Amazon's area. This is due in part to the capture of synthetic aperture radar (SAR) data using the ERS sensor, as well as issues preventing scatterometer measurement. The ERS sensor was capable of running in either scatterometer or SAR mode, but not both at once. When SAR mode was enabled, no scatterometer measurements were possible. This is the case for much ERS-2's lifetime, leaving stretches where backscatter data for only small parts of the Amazon is available for analysis.

As with ASCAT, predictions from ERS data are based on a linear regression of σ^0 anomaly values and deforestation area. Figure 8.6 shows ERS backscatter anomaly is less than ASCAT anomaly for the same amount of pixel deforestation, limiting the effectiveness of the linear regression. This is likely a product of the coarser resolution of the sensor, causing backscatter from deforested and non-deforested pixels to "bleed into" one another, decreasing the difference between the two.

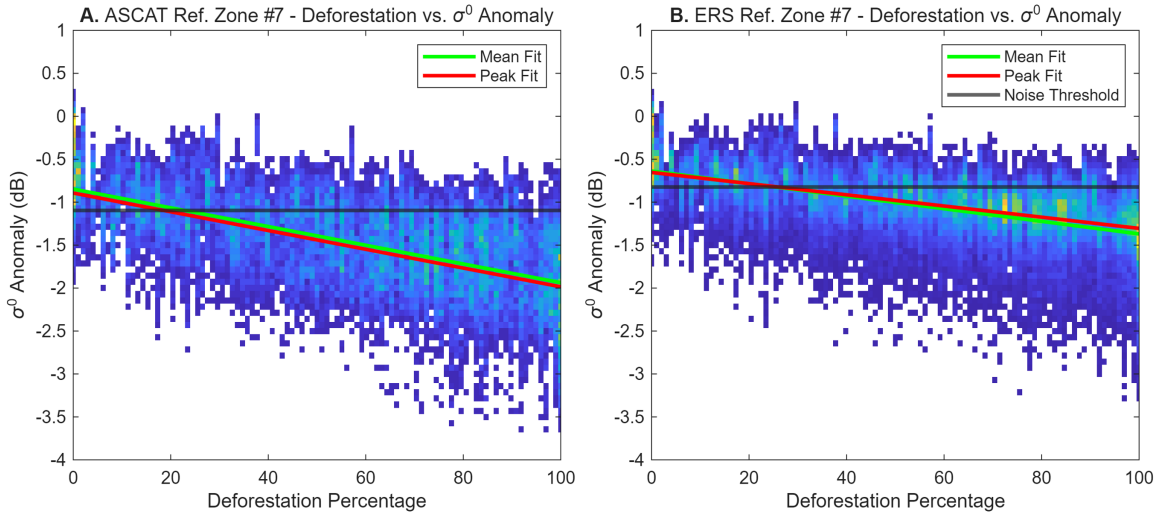

Figure 8.6: A scatter plot of deforestation and σ^0 anomaly data for ASCAT and ERS measurements in reference zone #2. Deforestation and protected study areas are consistent between both sensors, but the period of available data differs by several years. ASCAT deforestation data is sourced from combined PRODES and DETER deforestation alerts from 2016 to 2023, whereas ERS utilizes PRODES data from 2002 to 2011, as no DETER data is available during the operating period of ERS-2.

Finally, the concentration of deforestation in the study area plays a role in prediction accuracy. Low levels of deforestation differ less in brightness from non-deforested areas than high levels of deforestation. At the time that ERS operated, deforestation had not spread as much nor was it as complete as today (see Figure 6.1). Low levels of deforestation may fall below the noise threshold for the prediction regression, preventing meaningful conclusions from being made. Areas where concentrated deforestation did occur were generally not suitable for comparison between ASCAT and ERS, due to not being covered during the overlapping period of the two sensors, lacking a close enough protected biome, or being too close to major bodies of water.

While the rate of deforestation has slowed since ERS's service, it has accumulated significantly over time across the Amazon. With the present estimation approach, it is unlikely that poorly-concentrated deforestation areas can be reliably reconstructed using ERS data, but further validation may reveal other useful capabilities pertaining to the Amazon. Analog PRODES datasets not available digitally [5] overlap with the entirety

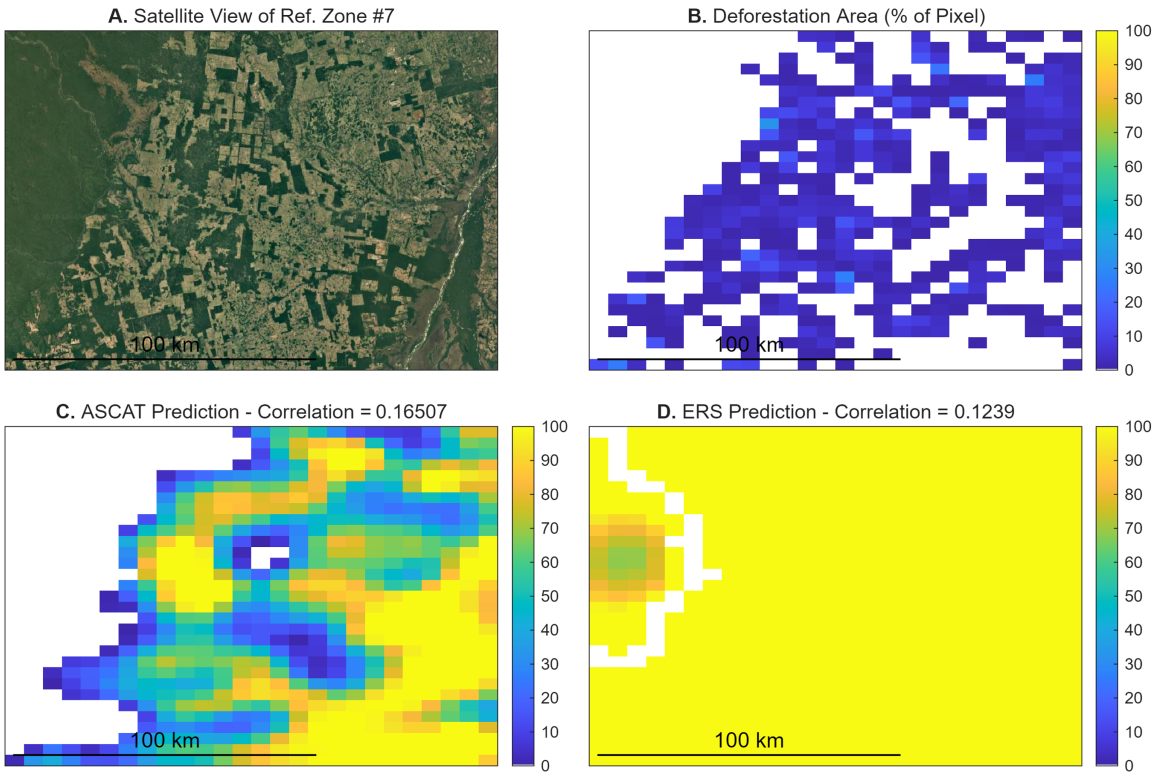

Figure 8.7: Deforestation predictions using ASCAT and ERS scatterometer data compared to *in situ* deforestation data. The satellite image shown in **A.** is provided by Google Earth historical imagery and shows the reference zone on December 31, 2011, the nearest available date.

of ERS's lifespan and would provide valuable insight into deforestation's impact on ERS backscatter. That said, the remarkable performance improvements of ASCAT over ERS, even for this unintended application of the data, further emphasize the advancements made in instrument design, calibration, and data processing since ERS's conception.

8.4 Detector Performance

Detecting deforestation relies first and foremost on the accuracy of estimation in this methodology. Thus, if estimation proves inaccurate for a reference zone or climate, then it is unlikely that detection will be successful. A detector's performance may be considered an overview or simplification of the abilities of its respective estimator, showing where its area and distribution estimates are "close enough" to be considered accurate.

With the exception of zone #5, all reference zone detectors performed measurably better than chance. The "mean" estimate generally showed better performance, as judged by distance from a perfect predictor, than "peak" regressions and is shown in the tables contained in this section. Correlation is generally lower for detectors as the penalty for misidentifying a pixel is higher than miscalculating its deforestation area. At a climate zone scale, detection was no better than or worse than random classification, except for in the tropical savanna climate zone. That said, it does not mean that the estimator fails to provide useful information. At this scale, visual inspection is a valuable tool to determine what estimations are reasonable. It is unlikely that a large contiguous region would experience consistent levels of deforestation, such as is seen in the Rio Negro region in the

Ref. Zone	Optimal Def. (δ)	Det. Rate ($\alpha(\delta)$)	FP Rate ($\beta(\delta)$)	Corr.	Dist.
1	8.4	82.2	28.1	0.689	0.333
2	42.7	86.9	18.8	0.663	0.228
3	22.4	88.1	10.3	0.771	0.157
4	7.0	86.1	12.5	0.763	0.187
5	0.1	52.2	14.0	0.343	0.498
6	2.1	86.8	17.7	0.478	0.220

Table 8.3: Optimum detector performance for reference zones using measurements taken July 2023. Note that optimal deforestation, detection rate, and false positive rate are percentages. As described in Equation 7.4, an optimal detector is defined as one with performance closest to the point of perfect detection.

northwest of Figure 8.4. While this region would be classified as deforested by the detector, a knowledgeable observer could reasonably disregard this prediction.

While the optimum detector is described in this section, a detector may be selected within the range of operation depending on performance requirements. By defining an acceptable false positive rate, a deforestation threshold can be defined that yields the highest rate of detection at that rate. For example, if one were to use the detector for reference zone #3 shown in Figure 8.8, setting a maximum false positive rate of 0.05, the most powerful detector would successfully identify deforestation for 81.2% of pixels. Or alternatively, a user might identify a desired detection rate, and would then choose the detector with that gives the fewest false positives. For example, if the user determined that they must detect at least 90% of deforested pixels, the minimum false positive rate would be approximately 0.129.

Ref. Zone	Climate	Optimal Def. (δ)	Det. Rate ($\alpha(\delta)$)	FP Rate ($\beta(\delta)$)	Dist.
1	Aw	0.1	65.0	10.9	0.367
2	Aw	19.2	85.0	27.8	0.316
3	Am	0.0	100.0	50.0	0.500
4	Am	0.0	100.0	50.0	0.500
5	Af	0.1	58.0	23.1	0.480
6	Af	15.0	66.9	30.4	0.449

Table 8.4: Optimum detector performance for reference zones using measurements taken July 2023. Note that optimal deforestation, detection rate, and false positive rate are percentages. A distance close to 0.5 constitutes a failure of the detector, as it does not perform better than chance for identifying deforested pixels.

The detection rate chosen determines the likelihood of false positives and vice versa. Factors in determining the rate vary by use case, such as detector system requirements or the cost of misidentification. In the case of environmental policy enforcement, the cost of acting on a false positive might be substantial, such as sending a helicopter expedition to the remote Amazon without reason.

A binary detector is most useful in cases where there is a need for clear distinction between one state and the other. For example, optical data is used for the DETER projects because it is at a high enough resolution that a pixel would either be healthy or completely deforested, so the odds of misclassification are low. Thus, binary detection is sufficient to enable rapid response to any unexpected landscape-degrading activity. At the scale of C-band scatterometer data, it is unlikely that a large enough area of native vegetation would

be removed at once for detection and more likely that a false positive is given. Additionally, a pixel reaching the minimum threshold for detection still contains substantial vegetation, necessitating a range of values rather than a binary demarcation of deforestation.

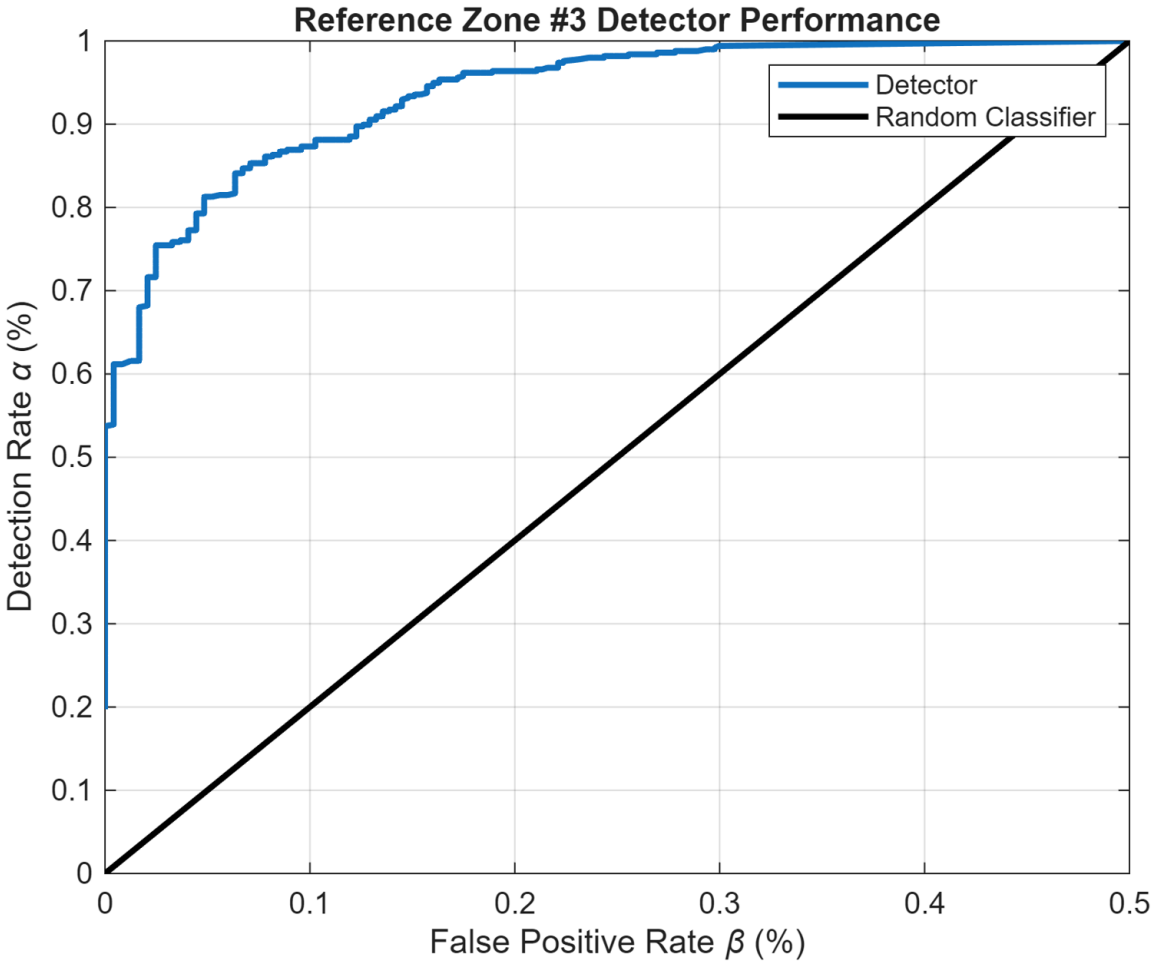

Figure 8.8: Receiver operating characteristic for reference zone #3. Minimum deforestation is set according to the noise threshold for this zone (see Table 8.1). The black line represents a random classifier, which assigns pixels as deforested or non-deforested by chance.

Therefore, given the realities of the problem of deforestation, a detector constructed using this methodology has limited usefulness for tracking rainforest health. Strong detector capability, however, is not a primary goal of this research, as the methodology is instead tailored to the problem of estimation. To optimize for detection, approaches oriented towards change detection are more appropriate, such as comparing between individual scatterometer images rather than monthly averages. That said, lackluster detector performance in no way detracts from the strengths this approach has for estimating deforestation area and distribution.

Overall, the results discussed demonstrate that this method successfully estimates deforestation in a wide range of circumstances. Provided a degree of familiarity with the measured environment, it highlights the patterns of land use, diversity of climates and vegetation, and impacts of human activity using a dataset that would normally not be employed for these purposes.

9 Conclusion

This research explores a previously unexamined application of C-band scatterometer data and demonstrates that it can be employed to estimate deforestation. This is accomplished with a high degree of accuracy at a local scale and performs acceptably when expanded across climate zones. Beyond that, it can be applied to a variety of vegetation types ranging from grassland to tropical rainforest.

Though there are many existing methods of tracking deforestation, the simplified classification model developed herein stands out for using C-band scatterometer measurements while relying on minimal contextual data to ease prediction and classification. This model has applications for estimating deforestation and landscape degradation in scenarios where microwave SAR data is not an option or where atmospheric conditions preclude the use of traditional optical processes.

The approach developed herein utilizes ASCAT UHR data to predict Amazon deforestation and is validated using a combination of PRODES and DETER tracking, but has applications beyond Brazil. Because the methodology is not dependent on external landscape classification, analysis can be done with scatterometer data alone. By selecting a stable reference area and an area to analyze for anomalies in σ^0, landscape degradation estimates can be obtained almost immediately by applying the appropriate regression. This is especially useful for highlighting areas of interest in vegetation studies and other exploratory applications.

At its core, this research shows that deforestation has a measurable and predictable impact on C-band backscatter. This has implications for scatterometer calibration, which is widely performed based on Amazon backscatter measurements. Because of the extent of deforestation and its increased rate in recent years, areas that were previously untouched may already be under threat of disruption or will be in the future. Beyond the direct environmental impact of human activities, there are also the indirect consequences of climate change in altered rainfall and temperature changes which will gradually impact Amazon vegetation over time. These factors must be taken into account when selecting calibration areas. The methodology developed herein may be useful for predicting the impact of deforestation on vegetation backscatter in calibration areas or for identifying new areas for consideration.

Due to obvious limitation in sensor resolution, the methodology may be further improved by using higher resolution data, such as 3.125 km ASCAT UHR data or measurements from other microwave sensors. Additionally, accurate estimation relies on the selection of properly representative reference zones. In this thesis, reference areas were selected using an ad-hoc process by identifying concentrated pockets of deforestation with protected areas nearby. Improved estimation accuracy could be achieved using a more systematic, automated approach to identify undisturbed pixels as a reference for those in the immediate vicinity. This would ensure similar vegetation and climate characteristics, rather than assuming protected areas serve as an adequate reference for an entire region. Alternatively, more fine-grained landscape classification could be used to identify what protected regions

might be applicable to an area. By pairing protected and deforested pixels using external landscape coverage data, one might avoid the wide misclassifications present in tropical monsoon (Am) and tropical rainforest (Af) climate estimates.

This methodology is suitable for comparing deforestation and backscatter on a single-month basis, but does not take into account previous measurements when making predictions. Future research may develop a modified analysis comparing pixel brightness over time to make temporally consistent predictions. The current method uses scatterometer measurements averaged over a single month, meaning that random backscatter variation may cause an individual pixel to jump in estimated deforestation value from month to month. Using detection-specific techniques such as constant false alarm rate (commonly known as CFAR), likely deforested pixels could be identified based on their change over time. For example, by defining an appropriate window of time to account for natural variance in backscatter over time, only significant changes to a pixel's brightness between measurements would trigger processing for deforestation. Alternatively, sophisticated spatiotemporal algorithms like Bayesian online change point detection [47] (for detection of rapid deforestation events) or BFAST decomposition [48] (for long time-term degradation trends) may be adapted for low-resolution scatterometer data. This would be most appropriate for periods not already covered by high-resolution sensors like C-band SAR satellites [4].

Finally, future research may expand on this approach to identify landscape degradation in tropical regions around the world. The Amazon rainforest is extensively studied and monitored, but rainforests and savannas in other parts of the world do not have the same resources dedicated to their protection. This methodology deliberately requires minimal additional information for landscape classification to ease its application to regions or periods of time where such contextual data may be unavailable. Assuming a small amount of *in situ* deforestation data is available for the desired study region, this methodology could be validated and applied to any tropical region. Then, a history of backscatter measurements would be used to create a timeline of land usage change, highlighting regions of interest for further study using high-resolution data.

The Amazon is a unique collection of ecosystems that has immense value for the world as a whole. Tropical forests and grasslands serve as keystones to global environmental and ecological processes, but beyond that they are significant to the people and cultures that call them home. If they are to be protected and responsibly managed, methods to study them that take into account their diversity and role in society must be developed and refined. This research represents a small contribution to the efforts being made to conserve the natural world for future generations.

References

[1] Hoang, N. T. and Kanemoto, K., "Mapping the deforestation footprint of nations reveals growing threat to tropical forests," *Nature Ecology & Evolution*, vol. 5, no. 6, March 2021, pp. 845–853. DOI: 10.1038/s41559-021-01417-z

[2] West, C., Rabeschini, G., Singh, C., Kastner, T., Bastos Lima, M., Dermawan, A., Croft, S., and Persson, U. M., "The global deforestation footprint of agriculture and forestry," *Nature Reviews Earth & Environment*, vol. 6, no. 5, 2025, pp. 325–341.

[3] Maurano, L. E., Queiroz, G. R., Vinhas, L., Ferreira, K. R., Almeida, C. A., and Costa, R. W., "DETER Intenso and forest monitor: Improving the alerting of deforestation in the Brazilian Amazon rainforest," *Anais do XX Simpósio Brasileiro de Sensoriamento Remoto*, April 2023.

[4] Doblas, J. *et al.*, "Optimizing near real-time detection of deforestation on tropical rainforests using Sentinel-1 data," *Remote Sensing*, vol. 12, no. 23, November 2020, p. 3922. DOI: 10.3390/rs12233922

[5] Shimabukuro, Y. E. *et al.*, *The Brazilian Amazon monitoring program: PRODES and DETER projects*, *Global Forest Monitoring from Earth Observation*, Cleveland, OH, USA: CRC Press, 2012, pp. 153–169.

[6] Sales, V. G. *et al.*, "Cloud cover and its impact on Brazil's deforestation satellite monitoring program: Evidence from the Cerrado biome of the Brazilian Legal Amazon," *Applied Geography*, vol. 140, March 2022, p. 102 651. DOI: 10.1016/j.apgeog.2022.102651

[7] Tilahun, Z. A., "The effects of human activities on Amazon Rainforest," *International Journal of Scientific Research in Civil Engineering*, vol. 3, no. 6, 2019, pp. 114–121.

[8] *Unidade de Conservação: Parque Nacional do Viruá*, Accessed 15 May 2026, 2026.URL: https://sistemas.mma.gov.br/cnuc/index.php?ido=relatorioparametrizado.exibeRelatorio&relatorioPadrao=true&idUc=179.

[9] *Flora and Fauna of the Amazon*, Accessed 2 June 2026, April 2026.URL: https://www.ispn.org.br/en/biomas/amazonia/fauna-e-flora-da-amazonia/.

[10] Carvalho, W. D. *et al.*, "Amazonian savannas are an integral part of Brazil's Amazon "biome": Implications for environmental policies," *Discover Conservation*, vol. 2, no. 1, March 2025. DOI: https://doi.org/10.1007/s44353-025-00031-5

[11] Balee, W., "Indigenous history and Amazonian biodiversity," *Changing tropical forests: Historical perspectives on today's challenges in central & south america*, 1992, pp. 233–251.

[12] Neves, E. G., "Archaeological cultures and past identities in the pre-Colonial Central Amazon," *Ethnicity in ancient Amazonian: Reconstructing past identities from Archaeology, Linguistic and Ethnohistory. Boulder: University Press of Colorado*, 2011, pp. 1–27.

[13] Cunha, M. C. d. and De Almeida, M. W., "Indigenous people, traditional people, and conservation in the Amazon," *Daedalus*, vol. 129, no. 2, 2000, pp. 315–338.

[14] Nascimento, M. N., Aukes, T. F., and McMichael, C. N., "Indigenous and Colonial influences on Amazonian forests," *Plants, People, Planet*, vol. 6, no. 4, 2024, pp. 803–823.

[15] Assunção, J. *et al.*, "DETER-ing deforestation in the Amazon: Environmental monitoring and law enforcement," *American Economic Journal: Applied Economics*, vol. 15, no. 2, April 2023, pp. 125–156. DOI: 10.1257/app.20200196

[16] Almeida, C. A. de *et al.*, "Methodology for forest monitoring used in PRODES and DETER projects," *CEP*, vol. 12, no. 010, 2021, pp. 3–2.

[17] Shimabukuro, Y. E., Santos, J. R. dos, Formaggio, A. R., Duarte, V., and Rudorff, B. F. T., *The Brazilian Amazon monitoring program: PRODES and DETER projects*, *Global forest monitoring from earth observation*, vol. 2012, CRC Press Boca Raton, FL, 2012, pp. 153–169.

[18] Singh, S. *et al.*, "The legacy of scatterometers: Review of applications and perspective," *IEEE Geoscience and Remote Sensing Magazine*, vol. 10, no. 2, June 2022, pp. 39–65. DOI: 10.1109/mgrs.2022.3145500

[19] *Wavelength*, *Encyclopedia Britannica*, Accessed 16 January 2026, January 2026.URL: https://www.britannica.com/science/wavelength.

[20] Bruder, J. A., "IEEE radar standards and the radar systems panel," *IEEE Aerospace and Electronic Systems Magazine*, vol. 28, no. 7, 2013, pp. 19–22.

[21] Lin, C.-C. *et al.*, "Three generations of C-band wind scatterometer systems from ERS-1/2 to MetOp/ASCAT, and MetOp second generation," *IEEE Journal of Selected Topics in Applied Earth Observations and Remote Sensing*, vol. 10, no. 5, May 2017, pp. 2098–2122. DOI: 10.1109/jstars.2016.2616166

[22] *SCIRoCCo - Earth Online*, https://earth.esa.int/eogateway/activities/scirocco, Accessed 3 April 2026, January 2017.

[23] Petchiappan, A. *et al.*, "The influence of vegetation water dynamics on the ASCAT backscatter–incidence angle relationship in the Amazon," *Hydrology and Earth System Sciences*, vol. 26, no. 11, June 2022, pp. 2997–3019. DOI: 10.5194/hess-26-2997-2022

[24] Long, D. G. and Skouson, G. B., "Calibration of spaceborne scatterometers using the Amazon tropical rainforest," vol. 1935, 1993, pp. 74–83.

[25] Wang, Y. *et al.*, "Understanding the radar backscattering from flooded and nonflooded Amazonian forests: Results from canopy backscatter modeling," *Remote Sensing of Environment*, vol. 54, no. 3, December 1995, pp. 324–332. DOI: 10.1016/0034-4257(95)00140-9

[26] Frolking, S. *et al.*, "Detection of large-scale forest canopy change in pan-tropical humid forests 2000–2009 with the SeaWinds Ku-band scatterometer," *IEEE Transactions on Geoscience and Remote Sensing*, vol. 50, no. 7, July 2012, pp. 2603–2617. DOI: 10.1109/tgrs.2011.2182516

[27] Wagner, W. *et al.*, "A study of vegetation cover effects on ERS scatterometer data," *IEEE Transactions on Geoscience and Remote Sensing*, vol. 37, no. 2, March 1999, pp. 938–948. DOI: 10.1109/36.752212

[28] Cui, D., Liang, S., and Wang, D., "Observed and projected changes in global climate zones based on Köppen climate classification," *Wiley Interdisciplinary Reviews: Climate Change*, vol. 12, no. 3, 2021, e701.

[29] Veldman, J. W. and Putz, F. E., "Grass-dominated vegetation, not species-diverse natural savanna, replaces degraded tropical forests on the southern edge of the Amazon basin," *Biological Conservation*, vol. 144, no. 5, May 2011, pp. 1419–1429. DOI: https://doi.org/10.1016/j.biocon.2011.01.011

[30] Early, D. S. and Long, D. G., "Image reconstruction and enhanced resolution imaging from irregular samples," *IEEE Transactions on Geoscience and Remote Sensing*, vol. 39, no. 2, 2002, pp. 291–302.

[31] Long, D. G. and Early, D. S., "Enhanced-resolution ERS-1 scatterometer imaging with irregular samples," *Image Reconstruction and Restoration II*, vol. 3170, SPIE, 1997, pp. 140–149.

[32] Lindsley, R. D. and Long, D. G., "Enhanced-resolution reconstruction of ASCAT backscatter measurements," *IEEE Transactions on Geoscience and Remote Sensing*, vol. 54, no. 5, May 2016, pp. 2589–2601. DOI: 10.1109/tgrs.2015.2503762

[33] Hutchings, N. L., *Near-Coastal Ultrahigh Resolution Scatterometer Winds*. Brigham Young University, 2019.

[34] Lindsley, R. D., *Enhanced-resolution processing and applications of the ASCAT scatterometer*. Brigham Young University, 2015.

[35] Long, D. G. and Hardin, P. J., "Vegetation studies of the Amazon Basin using enhanced resolution Seasat scatterometer data," *IEEE Transactions on Geoscience and Remote Sensing*, vol. 32, no. 2, 2002, pp. 449–460.

[36] Long, D. G., Hardin, P. J., and Whiting, P. T., "Resolution enhancement of spaceborne scatterometer data," *IEEE Transactions on Geoscience and Remote Sensing*, vol. 31, no. 3, 2002, pp. 700–715.

[37] *MERS - Scatterometer and Radiometer Data Sets*, https://www.scp.byu.edu/data.html, Accessed 14 April 2026.

[38] *Bosque y Pérdida de Bosque*, Accessed 3 April 2026, 2024.URL: https://geobosques.minam.gob.pe/geobosque/view/perdida.php.

[39] *Inventario Forestal Nacional (IFN)*, Accessed 3 April 2026, 2021.URL: https://www.ideam.gov.co/nuestra-entidad/ecosistemas-e-informacion-ambiental/sistema-nacional-de-informacion-forestal-ifn.

[40] Beck, H. E. *et al.*, "High-resolution (1 km) Köppen-Geiger maps for 1901–2099 based on constrained CMIP6 projections," en, *Sci. Data*, vol. 10, no. 1, October 2023, p. 724.

[41] Souza, C. M. *et al.*, "Reconstructing three decades of land use and land cover changes in Brazilian biomes with Landsat archive and Earth Engine," *Remote Sensing*, vol. 12, no. 17, January 2020, p. 2735. DOI: https://doi.org/10.3390/rs12172735

[42] *TerraBrasilis - PRODES and DETER Download Files*, https://terrabrasilis.dpi.inpe.br/en/download-files/, Accessed 3 April 2026.

[43] Wagner, W., Scipal, K., Pathe, C., Gerten, D., Lucht, W., and Rudolf, B., "Evaluation of the agreement between the first global remotely sensed soil moisture data with model and precipitation data," *Journal of Geophysical Research: Atmospheres*, vol. 108, no. D19, 2003. DOI: https://doi.org/10.1029/2003jd003663

[44] Gallager, R. G., *Discrete Stochastic Processes*. Springer, October 1995.

[45] Scharf, L. L. and Demeure, C., *Statistical Signal Processing: Detection, Estimation, and Time Series Analysis*. Prentice Hall, 1991, pp. 105–109.

[46] *Parque Nacional do Viruá*, Accessed 15 May 2026, 2019.URL: https://www.gov.br/icmbio/pt-br/assuntos/biodiversidade/unidade-de-conservacao/unidades-de-biomas/amazonia/lista-de-ucs/parna-do-virua/informacoes-sobre-visitacao-2013-parna-do-virua.

[47] Bottani, M., Ferro-Famil, L., Poccard-Chapuis, R., and Polidori, L., "Continuous monitoring of fire-induced forest loss using Sentinel-1 SAR time series and a Bayesian method: A case study in Paragominas, Brazil," *Remote Sensing*, vol. 17, no. 16, 2025, p. 2822.

[48] Geng, L., Che, T., Wang, X., and Wang, H., "Detecting spatiotemporal changes in vegetation with the BFAST model in the Qilian mountain region during 2000–2017," *Remote Sensing*, vol. 11, no. 2, 2019. DOI: 10.3390/rs11020103

Appendices

A Reference Zone Comparisons

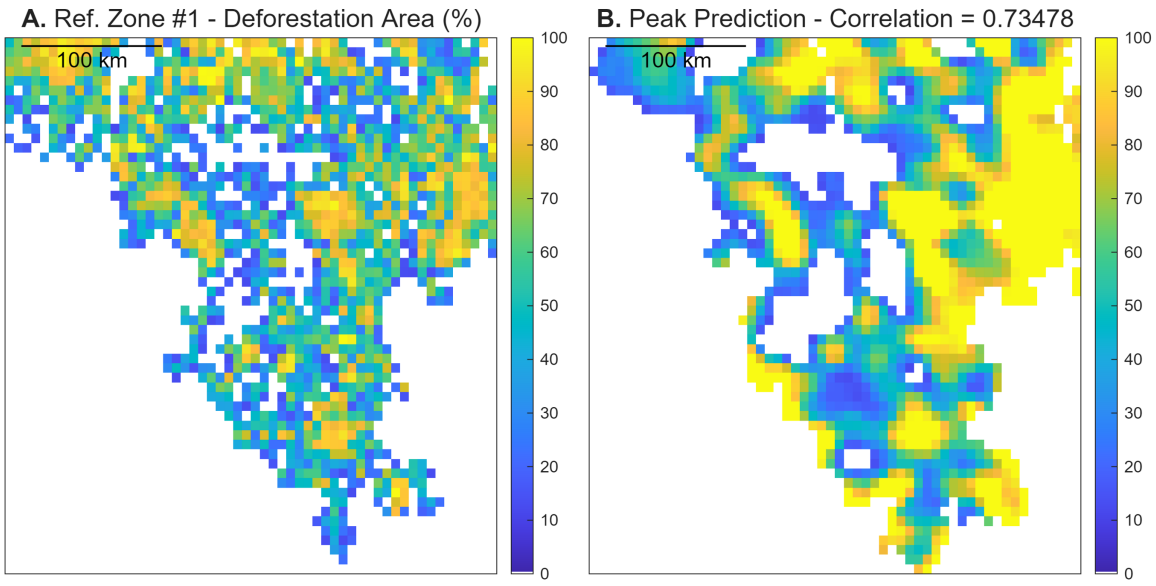

Figure A.1: *In situ* deforestation and deforestation prediction made using ASCAT measurements dating July 2023. The predictive regression is derived from accumulated deforestation measurements and σ^0 anomaly values in reference zone #1, surrounding Colíder, Mato Grosso.

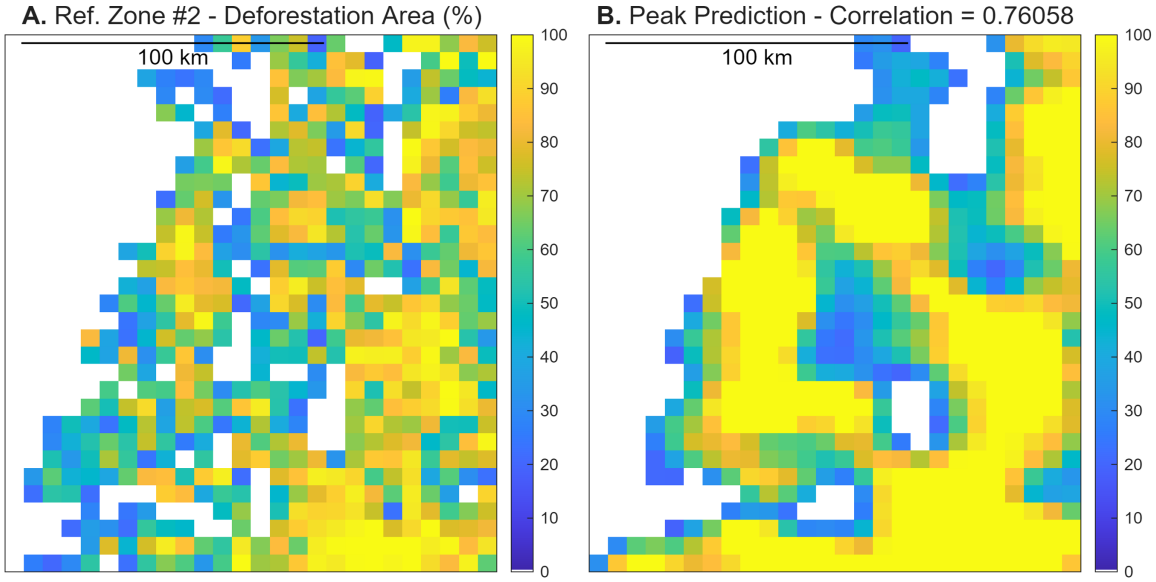

Figure A.2: *In situ* deforestation and deforestation prediction made using ASCAT measurements dating July 2023. The predictive regression is derived from accumulated deforestation measurements and σ^0 anomaly values in reference zone #2, surrounding Santana do Araguaia, Pará.

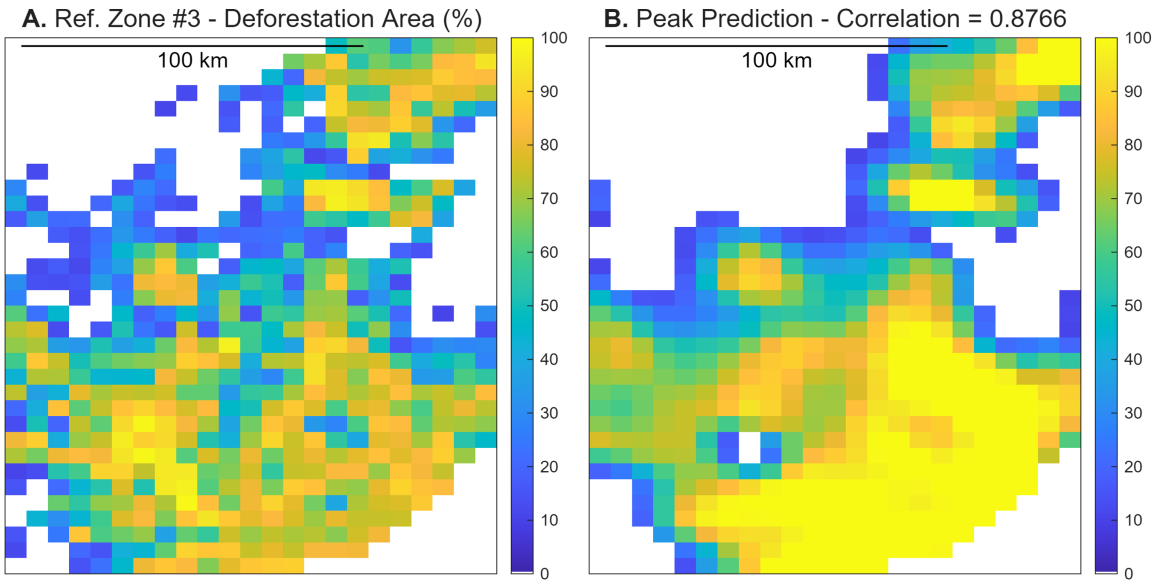

Figure A.3: *In situ* deforestation and deforestation prediction made using ASCAT measurements dating July 2023. The predictive regression is derived from accumulated deforestation measurements and σ^0 anomaly values in reference zone #3, surrounding Rio Branco, Acre.

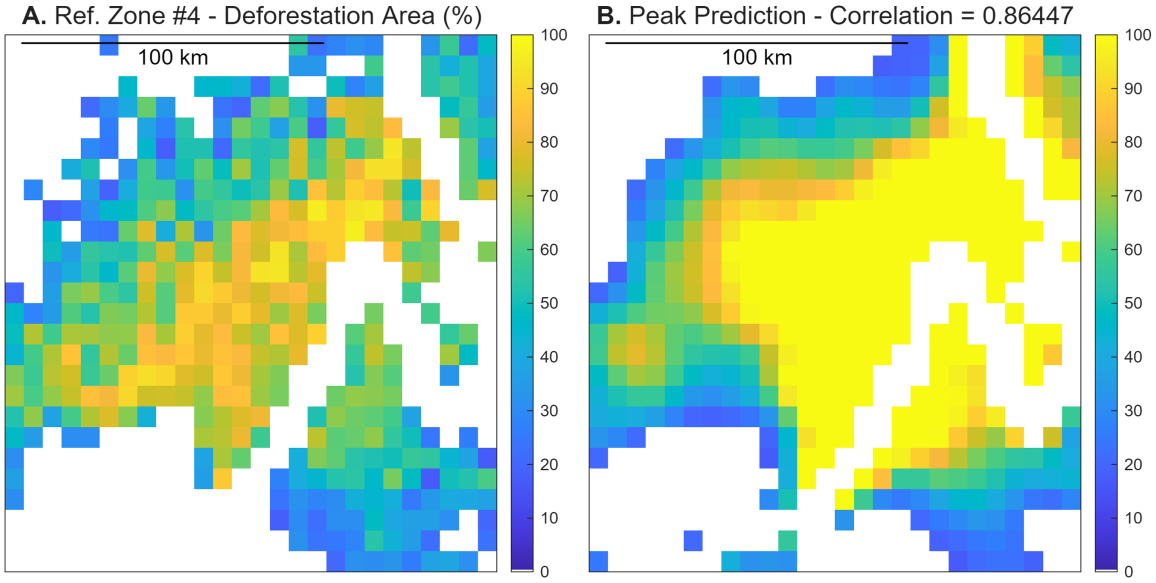

Figure A.4: *In situ* deforestation and deforestation prediction made using ASCAT measurements dating July 2023. The predictive regression is derived from accumulated deforestation measurements and σ^0 anomaly values in reference zone #4, surrounding Altamira, Pará.

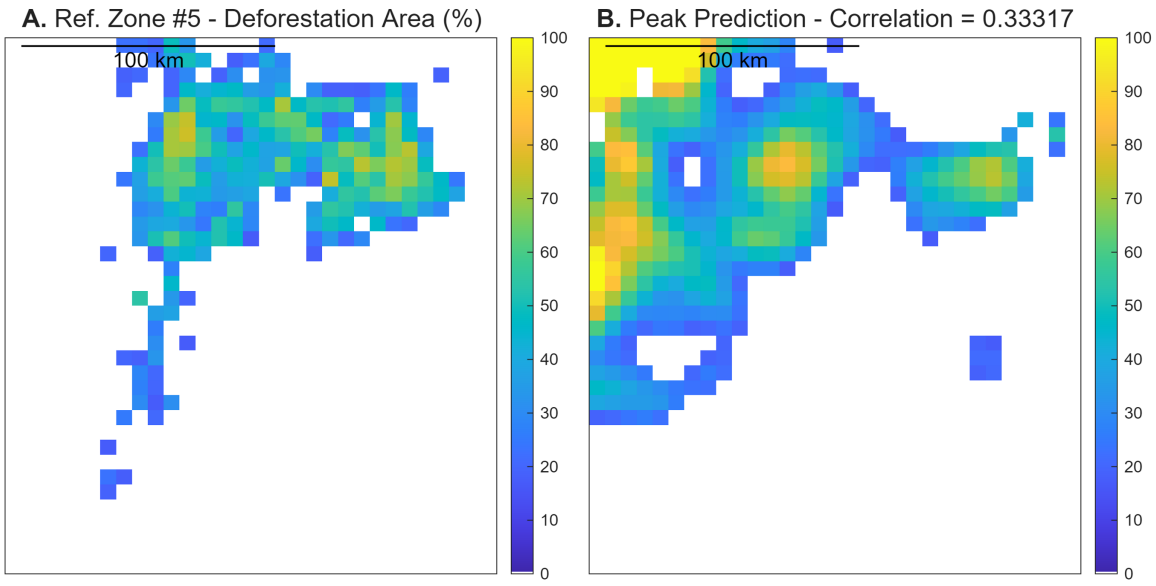

Figure A.5: *In situ* deforestation and deforestation prediction made using ASCAT measurements dating July 2023. The predictive regression is derived from accumulated deforestation measurements and σ^0 anomaly values in reference zone #5, surrounding Rorainópolis, Roraima.

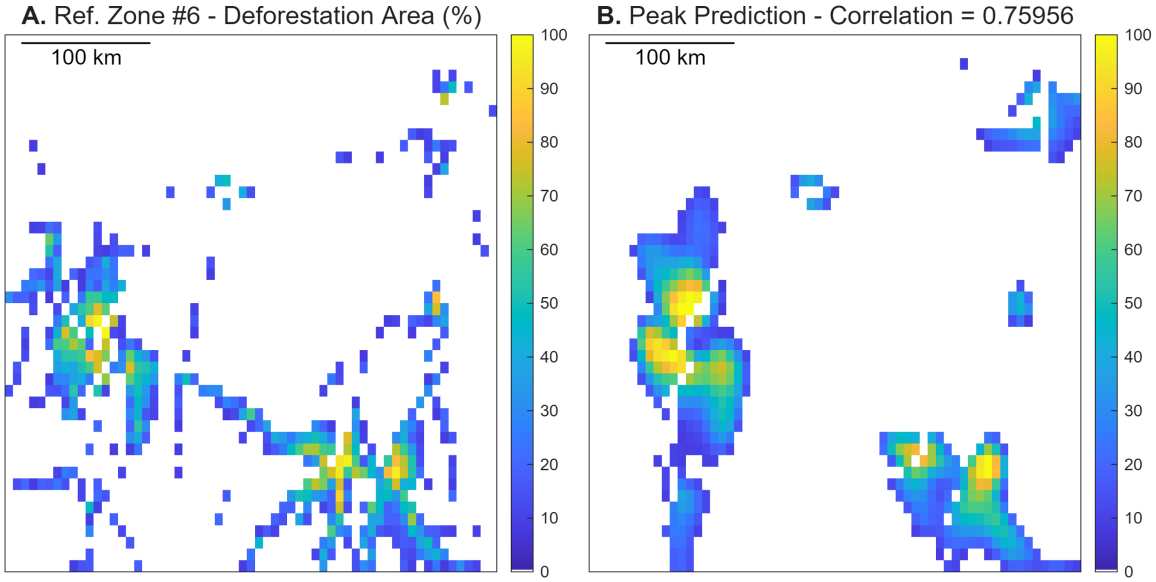

Figure A.6: *In situ* deforestation and deforestation prediction made using ASCAT measurements dating July 2023. The predictive regression is derived from accumulated deforestation measurements and σ^0 anomaly values in reference zone #6, surrounding Ipixuna, Amazonas.

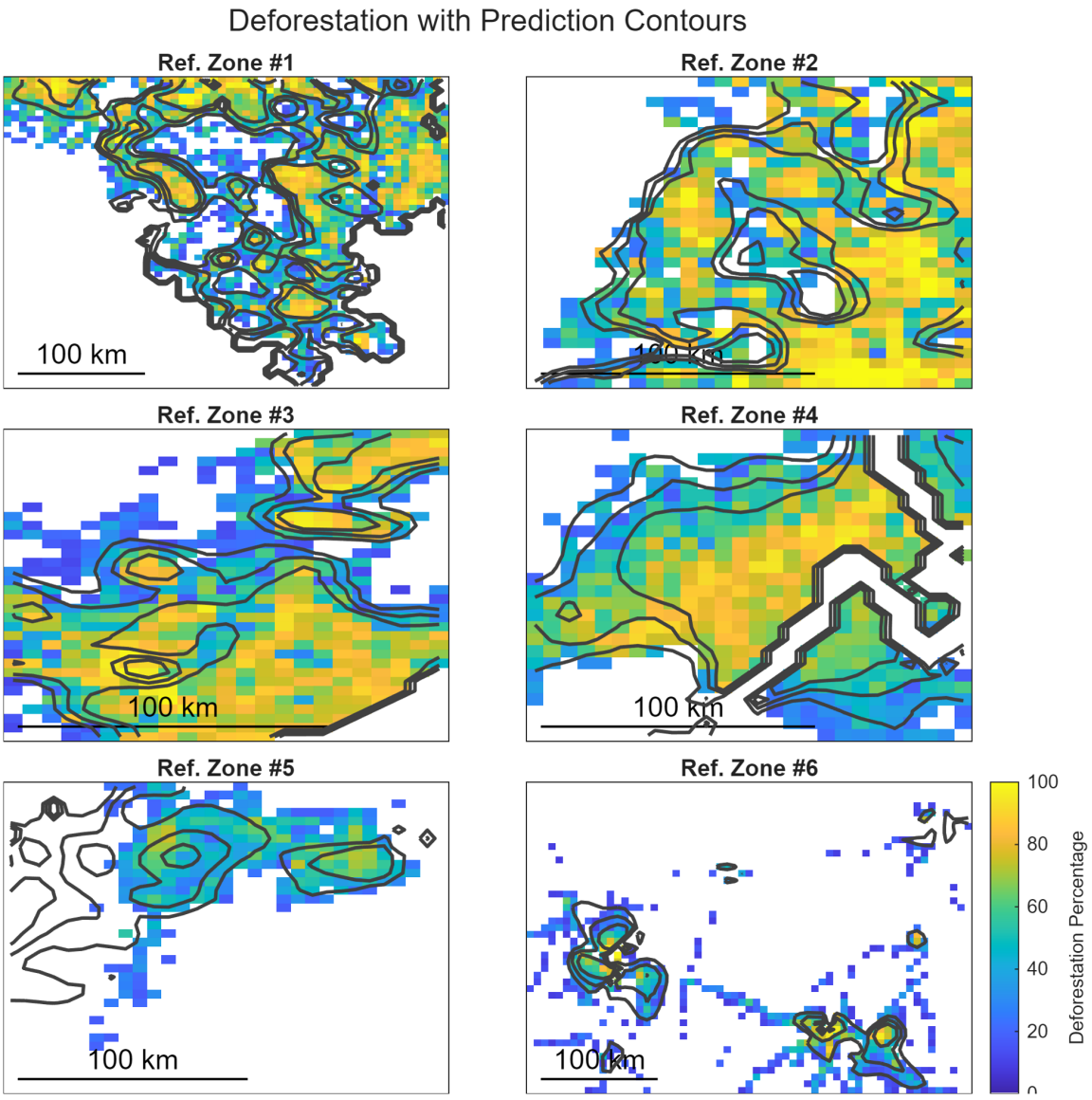

Figure A.7: *In situ* deforestation measurements with "peak" predictions overlaid as contour plot. Contour lines are set at 25%, 50%, and 75% deforestation. This visualization shows that, with the exception of reference zone #5, the predictions follow the broad patterns of deforestation very closely in each study area.

B Climate Zone Comparisons

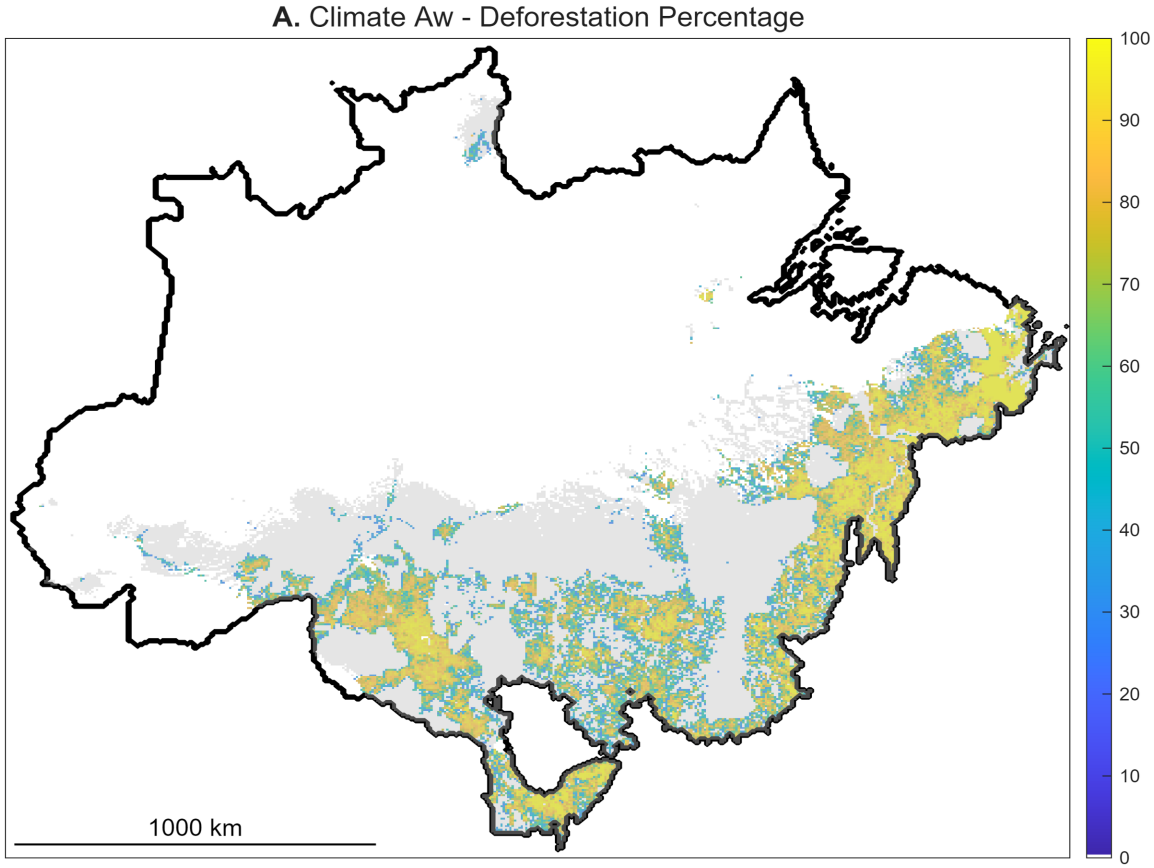

Figure B.1: Accumulated deforestation in tropical savanna climate zone (Aw) measured July 2023.

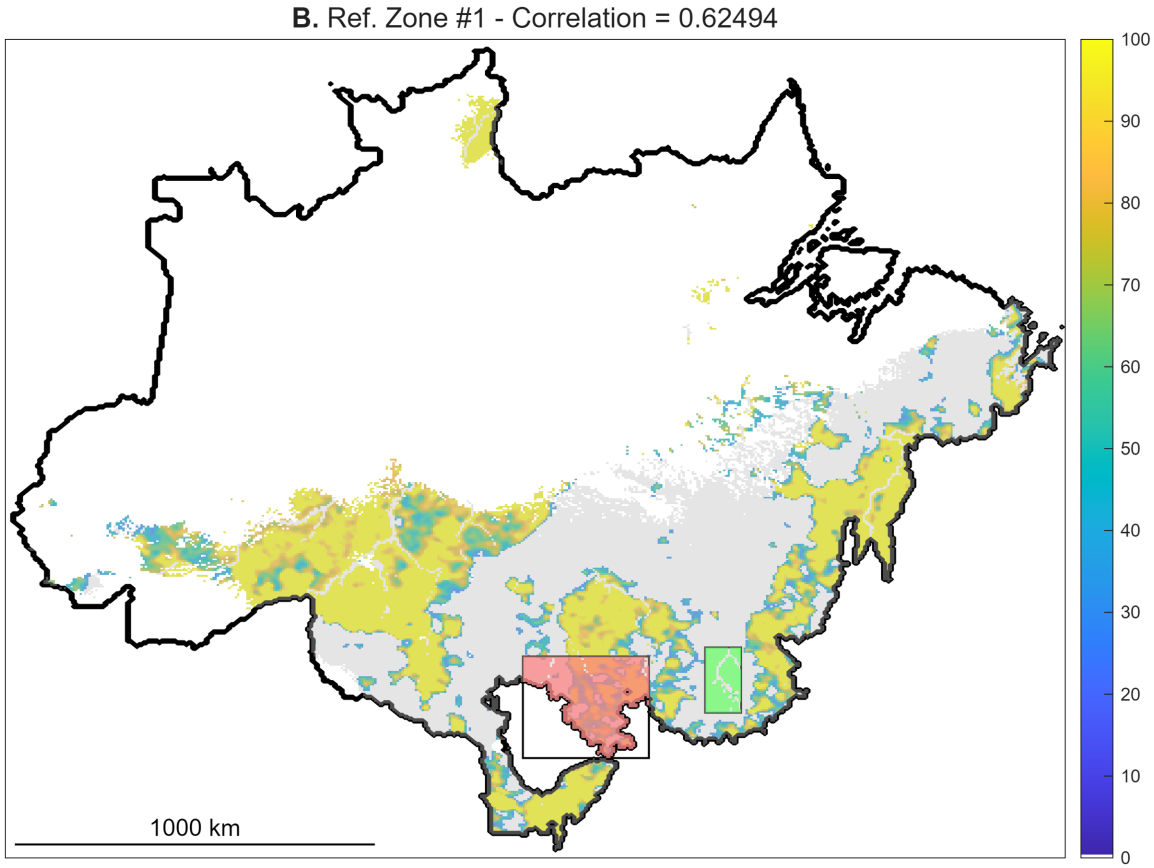

Figure B.2: Deforestation prediction for tropical savanna climate zone (Aw) from July 2023 ASCAT measurements. The predictive regression is derived from accumulated deforestation measurements and σ^0 anomaly values in reference zone #1, surrounding Colíder, Mato Grosso (shown in red).

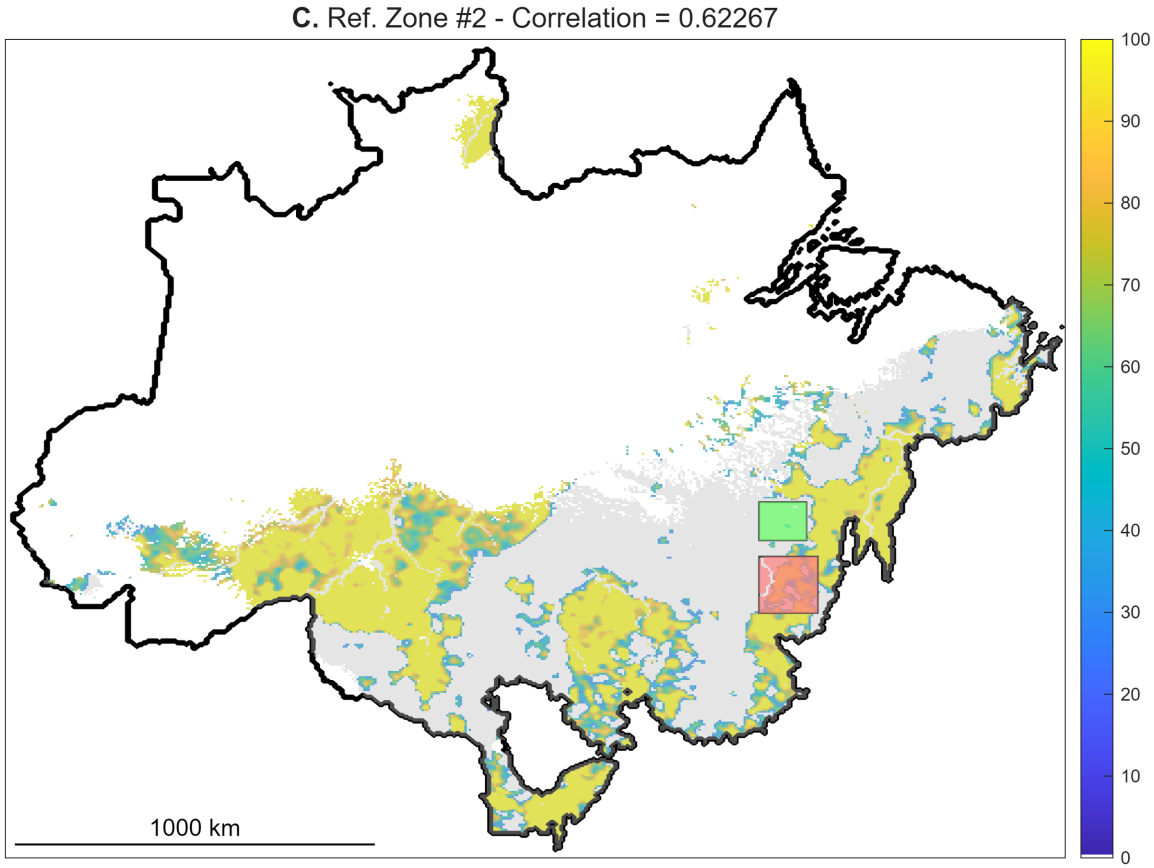

Figure B.3: Deforestation prediction for tropical savanna climate zone (Aw) from July 2023 ASCAT measurements. The predictive regression is derived from accumulated deforestation measurements and σ^0 anomaly values in reference zone #2, surrounding Santana do Araguaia, Pará (shown in red).

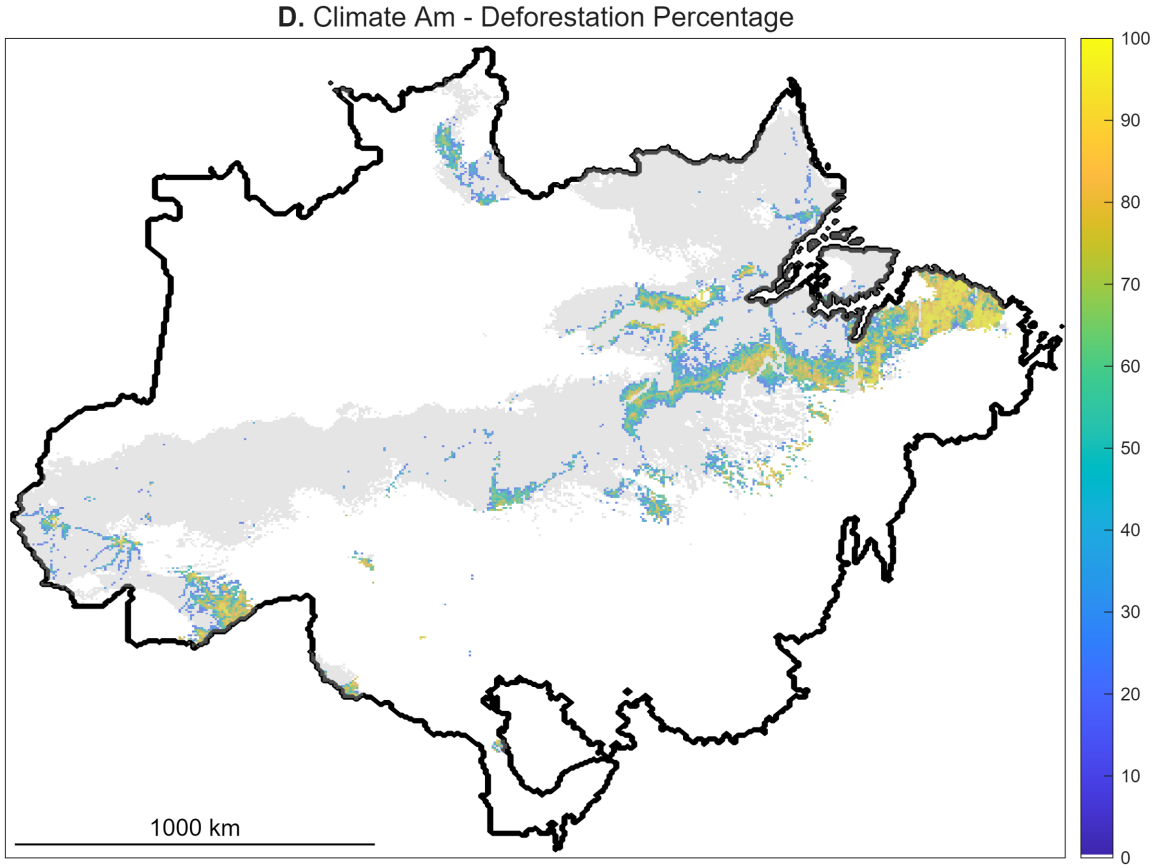

Figure B.4: Accumulated deforestation in tropical monsoon climate zone (Am) measured July 2023.

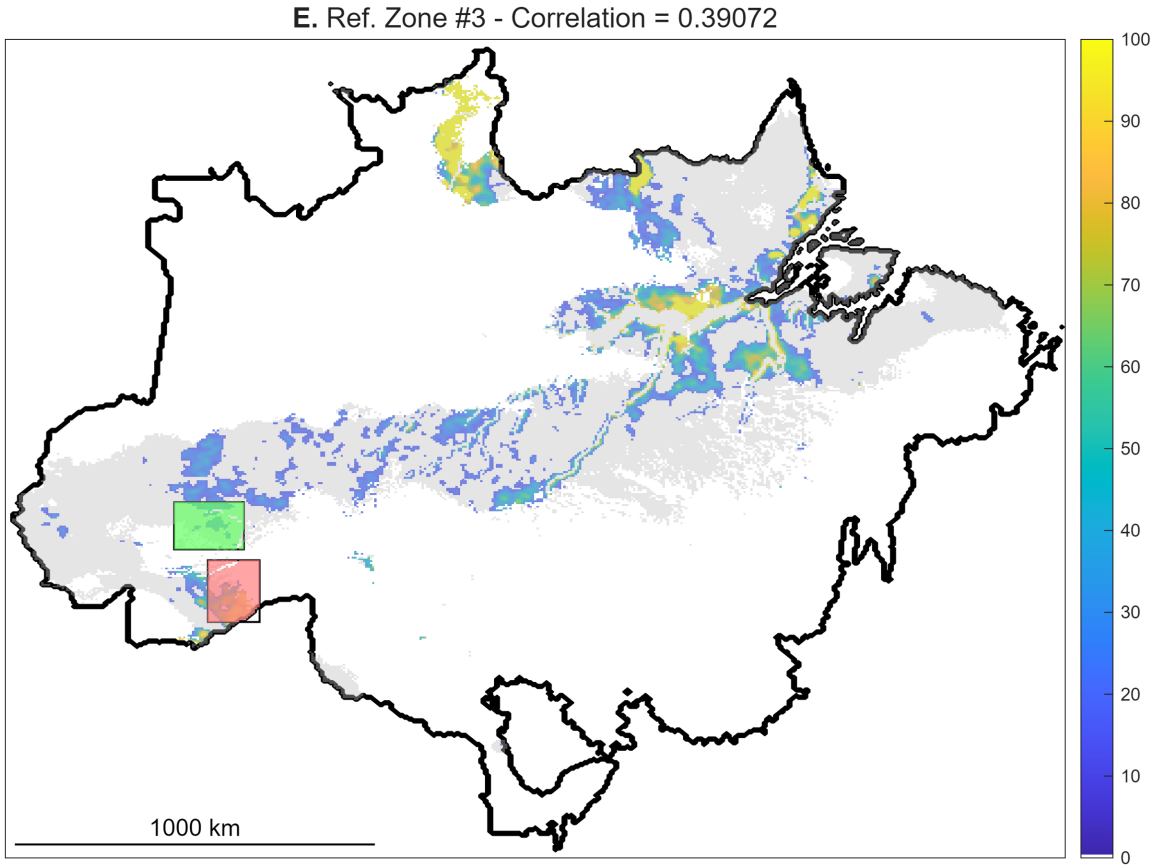

Figure B.5: Deforestation prediction for tropical monsoon climate zone (Am) from July 2023 ASCAT measurements. The predictive regression is derived from accumulated deforestation measurements and σ^0 anomaly values in reference zone #3, surrounding Rio Branco, Acre (shown in red).

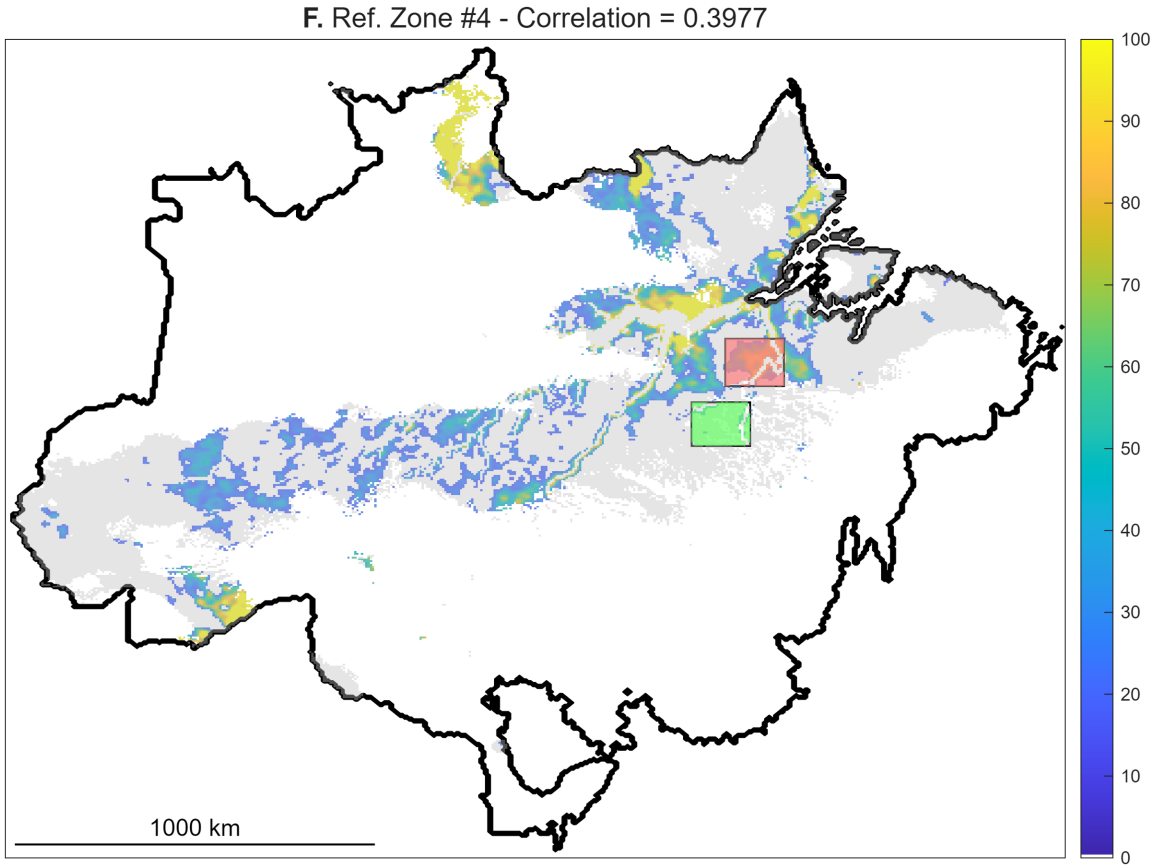

Figure B.6: Deforestation prediction for tropical monsoon climate zone (Am) from July 2023 ASCAT measurements. The predictive regression is derived from accumulated deforestation measurements and σ^0 anomaly values in reference zone #4, surrounding Altamira, Pará (shown in red).

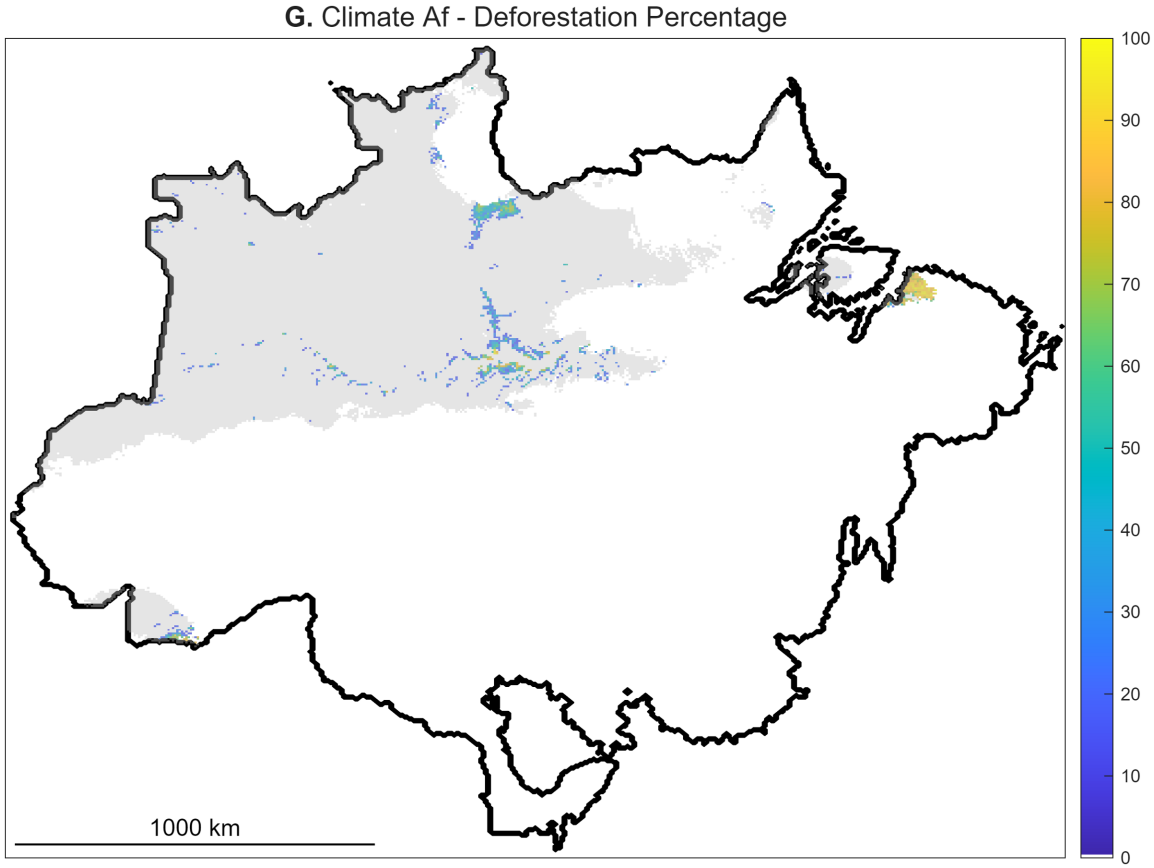

Figure B.7: Accumulated deforestation in tropical rainforest climate zone (Am) measured July 2023.

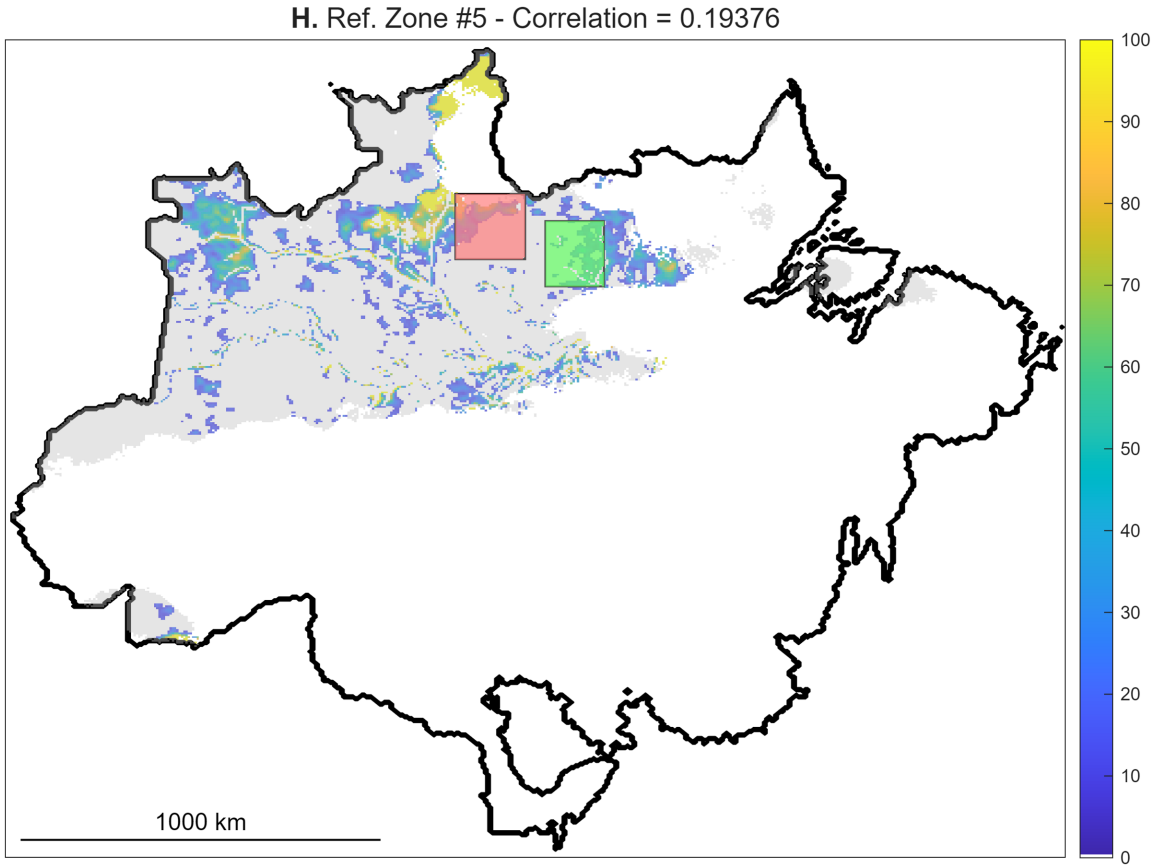

Figure B.8: Deforestation prediction for tropical rainforest climate zone (Af) from July 2023 ASCAT measurements. The predictive regression is derived from accumulated deforestation measurements and σ^0 anomaly values in reference zone #5, surrounding Rorainópolis, Roraima (shown in red).

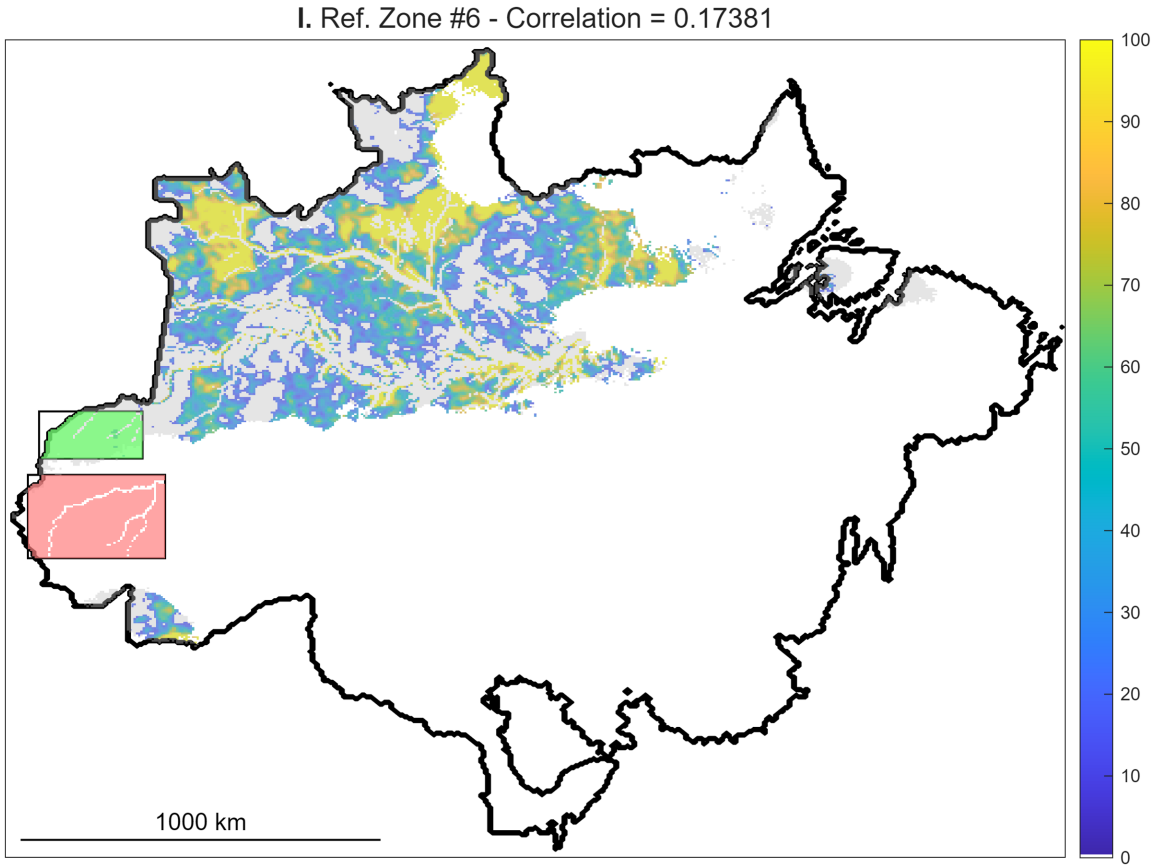

Figure B.9: Deforestation prediction for tropical rainforest climate zone (Af) from July 2023 ASCAT measurements. The predictive regression is derived from accumulated deforestation measurements and σ^0 anomaly values in reference zone #6, surrounding Ipixuna, Amazonas (shown in red).